Int. J. Solids Structures Vol. 30, No. 20, pp. 2779–2811, 1993
Printed in Great Britain

0020–7683/93 $6.00+ .00
Pergamon Press Ltd

FORMULATION, IDENTIFICATION AND USE OF INTERFACE MODELS IN THE NUMERICAL ANALYSIS OF COMPOSITE DELAMINATION

ALBERTO CORIGLIANO
Department of Structural Engineering, Politecnico of Milano, Piazza Leonardo da Vinci, 32, 20133 Milano, Italy

(*Received* 9 *October* 1992; *in revised form* 19 *March* 1993)

Abstract—Interface models which relate tractions to displacement jumps and which can be used to simulate fracture processes are formulated. The formulation and identification of the models are pursued with particular reference to the analysis of composite delamination. The difficulties concerning the use of interface models in numerical analyses are discussed. A numerical integration method for the interface constitutive laws is proposed, and the related consistent tangent modulus is derived. An algorithm for the structural analysis in the presence of softening interfaces which makes use of a local control condition is presented.

1. INTRODUCTION

The loss of cohesion between two solids can be thought of as the process in which the possibility to transfer tension and shear stresses between the two solids progressively diminishes. This damage phenomenon can be modelled by the introduction of *interface constitutive laws* in which the traction vector on the separation surface between the two solids is related to their reciprocal movement with respect to a reference configuration, i.e. to the displacement jump vector. For instance, if the stress component normal to the separation surface is a decreasing function of the distance between the two solids, the loss of cohesion will be complete when the stress reaches the zero for a critical distance.

Interface constitutive laws have been mainly used in the study of contact problems, fracture mechanics for concrete [see e.g. Hillerborg *et al.* (1976), Bažant and Oh (1983), Cedolin *et al.* (1987), Carpinteri (1989) and Maier *et al.* (1991, 1992)], adhesive films [among recent works on this subject see e.g. Frémond (1987) and Lemaitre (1992)], homogenized behaviour of composites [see e.g. Lene (1986) and Hashin (1990)] and of composite delamination. Their use and in particular the existence of a displacement discontinuity can be motivated in different ways, depending on the application envisaged.

In this paper interface models will be discussed in particular with reference to composite delamination, i.e. the phenomenon of separation of adjacent layers in laminated composites due to edge effects, impacts and other causes which originate important interfacial stresses [see e.g. Bottega (1983), Garg (1988) and Pagano (1989), and the references there listed].

The use of interface models in the analysis of composite delamination has been proposed by Allix (1989), and developed in Allix *et al.* (1991), Ladevèze (1992), Allix and Ladevèze (1992) and Daudeville (1992). In these works the schematization of the laminated composite proposed by Ladevèze (1986) is used. The laminated composite is conceived as an assemblage of two main constituents: the fibre-reinforced layer and separation interfaces. The attribution to these of an interface constitutive law allows the modelling of delamination, i.e. of progressive loss of cohesion between adjacent layers. Use of the same kind of idealization has been made in other recent works (Schellekens and de Borst, 1991, 1992).

The identification of interface models for composite delamination is complicated by the fact that experiments cannot be directly done on the interface, hence indirect information must be derived from tests. The kind of model which has to be used is generally characterized by anisotropy, softening and irreversibility. These features originate the main difficulties connected with the use of interface models in numerical analyses. As is well known, numerical analyses in the presence of softening deserve special care. Nonuniqueness of solutions and localization problems can completely falsify the results. Moreover, the local

softening behaviour can result in a global softening and also in snap-back phenomena that cannot be tackled with a standard step-by-step algorithm.

The purpose of this paper is to generalize the formulation of already existing interface models and to overcome some of the difficulties related to their use. In particular the problems of model identification, of numerical integration of the interface laws and of global analyses in the presence of softening interfaces are treated.

An outline of the paper is as follows. In Section 2 a formulation of a quite general class of interface models is presented. The models can be considered as particular manifestations of anisotropic softening plasticity, damage mechanics and coupled elasto-plasticity-damage theories [see e.g. Ladevèze (1983, 1986), Lemaitre (1984), Lemaitre and Chaboche (1985), Simo and Ju (1987) and Ju (1989)]. In Section 3 a discussion on energetic aspects concerning the process of delamination as modelled by an interface law is made. This permits the establishment of a clear link with classical Fracture Mechanics concepts. In Section 4 results of the discussion of Section 3 are used to propose an identification procedure for the models. Section 5 is dedicated to the analysis of the numerical integration of interface constitutive laws with the *backward difference* scheme. The consistent tangent operator is also given for a particular class of models [on this subject see e.g. Simo and Taylor (1985), Benallal *et al.* (1988), Perego (1988) and Comi *et al.* (1991)]. In Section 6 an algorithm for the solution of a boundary value problem for a solid which contains *softening interfaces* is presented. The algorithm makes use of an idea proposed by Chen and Schreyer (1990). Numerical examples are given in Section 7.

2. INTERFACE MODELS

Consider a surface Γ which separates two solids or divides a solid in two parts. The two parts will be called Ω_+ and Ω_-. Fix a point P on the surface Γ and introduce a local right handed reference frame 1, 2, 3 centred on P. Axis 3 is made coincident with the normal on Γ in P directed toward Ω_+ (Fig. 1). $\mathbf{t}$ is the three-components vector of tractions in P; the components of $\mathbf{t}$ will be considered positive if directed as axes 1, 2, 3. Suppose that displacement discontinuities can develop at point P belonging to surface Γ. The displacement vector $\mathbf{u}$ of point P thought to belong to Ω_+ or Ω_- will be denoted as $\mathbf{u}^+$ and $\mathbf{u}^-$, respectively. Denote by the symbol $[\mathbf{u}]$ the displacement jump vector in P, i.e. $[\mathbf{u}] \equiv \mathbf{u}^+ - \mathbf{u}^-$. An *interface constitutive law* is here defined as a relation between $\mathbf{t}$ and $[\mathbf{u}]$, i.e.

$$\mathbf{t} = A([\mathbf{u}], \mathbf{x}). \tag{1}$$

In eqn (1) A is an unspecified operator which connects displacement jumps to surface tractions in point P; $\mathbf{x}$ is a vector of *internal variables*.

When applied to the modelling of delamination in stratified composites, interface models have to possess the following main features: (a) the possibility of modelling a decrease in resistance (*softening*) until a critical level $[\mathbf{u}]_c$ is reached and the layers are completely separated; (b) the anisotropy of the response; (c) the difference in tensile and compressive behaviour for the direction normal to the surface (*unilateral effect*). Other

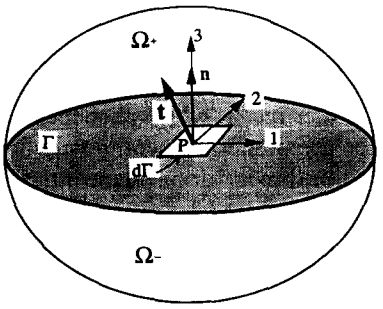

Fig. 1. Discontinuity interface Γ and local reference frame.

features which are important but not crucial can be introduced in the model: a decrease in stiffness, the existence of irreversible displacement discontinuities, time dependent behaviour. Another point to consider is the possible dependence of the interface behaviour on the orientation of fibers of adjacent layers (Laksimi *et al.*, 1991). A first way to take this into account is to define a local reference system of *principal directions* which depends on the orientation of fibres of adjacent layers (Allix, 1989). For instance, define a reference frame by taking as the principal direction 1 (or 2) the bisectrix of the angle formed by the direction of fibers of adjacent layers.

The development of displacement discontinuities, in the present context of composite delamination, corresponds to the development of a fracture. The definitions usually assumed in Fracture Mechanics of different modes can therefore also be used with reference to an interface law. Throughout the paper mode I (*opening mode*) will correspond to nonzero displacement discontinuities in direction 3 orthogonal to the interface, mode II and mode III (*shearing* and *tearing modes*) will be conventionally attributed to directions 1 and 2, respectively.

A general class of interface models, which generalizes the models proposed for delamination by Schellekens and de Borst (1991, 1992), and more particularly by Allix (1989), Allix and Ladevèze (1992), Daudeville (1992) and Ladevèze (1992) is expressed by the following relations, in which indices 1, 2, 3, refer to local principal directions of interface:

$$[\mathbf{u}] = [\mathbf{u}]^{\mathrm{e}} + [\mathbf{u}]^{\mathrm{p}}, \tag{2}$$

$$E = \{\tfrac{1}{2}(1-d_1)K_1[u_1]^{\mathrm{e}^2} + \tfrac{1}{2}(1-d_2)K_2[u_2]^{\mathrm{e}^2} + \tfrac{1}{2}(1-d_3)K_3^{+}\langle[u_3]^{\mathrm{e}}\rangle_{+}^{2} + \tfrac{1}{2}K_3^{-}\langle[u_3]^{\mathrm{e}}\rangle_{-}^{2} + \Psi(\eta)\}, \tag{3}$$

$$t_i = \frac{\partial E}{\partial [u_i]^{\mathrm{e}}} \quad i = 1,2,3, \quad Y_i = -\frac{\partial E}{\partial d_i} \quad i = 1,2,3, \quad \chi = \frac{\partial E}{\partial \eta} \equiv h(\eta), \tag{4}$$

$$F = F(t_i, Y_i, \chi; d_i), \quad G = G(t_i, Y_i, \chi; d_i), \tag{5}$$

$$[\dot{u}_i]^{\mathrm{p}} = \frac{\partial G}{\partial t_i}\dot{\lambda} \quad i = 1,2,3, \quad \dot{\eta} = -\frac{\partial G}{\partial \chi}\dot{\lambda}, \tag{6}$$

$$\dot{d}_i = l_i(t_i, Y_i, \chi; d_i)\dot{\lambda} \quad i = 1,2,3, \tag{7}$$

$$F \leqslant 0, \quad F\dot{\lambda} = 0, \quad \dot{\lambda} \geqslant 0. \tag{8}$$

Equation (2) expresses the displacement discontinuities [**u**] as the sum of an *elastic* (reversible) part $[\mathbf{u}]^{\mathrm{e}}$ and a *plastic* (irreversible) one $[\mathbf{u}]^{\mathrm{p}}$. In eqn (3) the free energy per unit surface E in isothermal conditions is given by the sum of two contributions. The first one is the elastic deformation energy per unit surface (the first four addends); d_i are damage variables, different for each direction 1, 2, 3 to take into account the anisotropy of damage evolution. K_i are *interface stiffnesses* with the dimension of a force over a length cube. The symbols $\langle\blacklozenge\rangle_+$ and $\langle\blacklozenge\rangle_-$ denote the positive and negative parts of $\blacklozenge$. These are introduced in relation (3) in order to take into account the unilateral effect. The second contribution $\Psi(\eta)$ of the free energy represents an energy per unit surface which depends on micromechanical rearrangements, Ψ is a function of the so-called kinematic internal variable η here assumed to be a scalar. Relations (4a, b, c) represent equations of state which define the variables conjugate to $[u_i]^{\mathrm{e}}$, d_i and η, respectively. Equation (4a) defines the tractions t_i as functions of elastic displacement discontinuities and damage variables. Notice that, in the principal reference frame here considered, t_i depends on the corresponding d_i and $[u_i]^{\mathrm{e}}$ only; notice also that a coupling between shear and normal tractions is never considered in the linear elastic relations even in nonprincipal reference frames. Equation (4b) defines the variables Y_i, conjugated to d_i, which have the dimension of an energy per unit surface. In eqn (4c) the static internal variable χ is defined as conjugated to η. Equations (5a) and

(5b) define the damage-yielding function F and the plastic potential G, respectively. The nonassociated evolution laws for plastic displacement discontinuities $[\mathbf{u}]^p$ and the kinematic internal variable η are given by eqns (6a) and (6b), respectively, $\dot{\lambda}$ is the *plastic-damage multiplier*. Equation (7) gives the evolution of damage variables. The loading–unloading conditions are given by relations (8). Note that, for the sake of simplicity, a single criterion F has been introduced for the development of damage and plasticity.

Relations (2)–(8) can be considered as the interface version of an elastic–plastic-damage constitutive model with nonassociated evolution laws for plastic variables and damage. The class of interface constitutive laws introduced possesses the main characteristics necessary to the modelling of composite delamination: anisotropic damage, unilateral effect, irreversible displacement discontinuities. Three noteworthy specializations will be discussed in the remaining part of this section.

2.1. *Model a: elastic–plastic-softening*

Consider the special choice:

$$l_i(t_i, Y_i, \chi; d_i) \equiv 0 \quad i = 1, 2, 3. \tag{9}$$

In this case the damage variables d_i are identically zero during the whole evolution, hence variables Y_i disappear too. The following expressions for the yielding function F and plastic potential G are chosen:

$$F = F(t_i, \chi) = f(a_1' t_1^2 + a_2' t_2^2 + a_3' \langle t_3 \rangle_+^2) + a_4' t_3 - \chi - 1, \tag{10}$$

$$G = G(t_i, \chi) = g(b_1' t_1^2 + b_2' t_2^2 + b_3' \langle t_3 \rangle_+^2) - \chi. \tag{11}$$

In the above equations f and g are positive convex and differentiable functions; $f(0) = g(0) = 0$; a_i', b_i', $i = 1, 2, 3$ and a_4' are non-negative model parameters.

Relations (2), (3) with $d_i = 0$, (4a, c), (6), (8), (10), (11) describe an elastic–plastic nonassociated class of models for the interface with isotropic hardening or softening. The behaviour is hardening for increasing function $h(\eta)$, softening for decreasing $h(\eta)$.

Consider the mechanical dissipation ω per unit surface:

$$\omega = \sum_{1}^{3} t_i [\dot{u}_i] - \dot{E} = \sum_{1}^{3} t_i [\dot{u}_i]^p - \chi \dot{\eta} \geq (g(t_i) - \chi)\dot{\lambda}. \tag{12}$$

Relation (12c) has been obtained by making use of: the evolution laws for $[\dot{u}_i]^p$ and $\dot{\eta}$, [eqns (6) and (11)], convexity and differentiability of g with respect to variables t_i, the fact that $g(0) = 0$. Notice that when $a_4 \equiv 0$, $g \equiv f$, and $a_i = b_i$, $i = 1, 2, 3$ (associated behaviour), relation (12c) together with (8) imply the non-negativeness of ω, thus satisfying a fundamental requirement of the second law of thermodynamics. In the case of nonassociated behaviour ($a_4' \neq 0$; $g \neq f$; $a_i' \neq b_i'$), the non-negativeness of ω is straightforwardly proved only for negative $\chi(\eta) = h(\eta)$, that is for ever decreasing resistance (softening) after yielding. In the general case of nonassociated law and static internal variable also positive, the requirement of positiveness of ω imposes some constraints on the choice of functions g, f and $h(\eta)$.

This model can take into account the decrease in resistance, the anisotropy, the unilateral effect and the presence of irreversible displacement discontinuities. The unilateral effect is introduced in such a way that pure compression in direction 3 does not cause yielding. Finally the linear term $a_4' t_3$ in the yielding function F [eqn (10)] delay yielding in the case of compression and accelerates it in the case of tension.

A particular member of the class of elastic–plastic-softening models here introduced will be considered for further discussion and numerical examples of Section 7:

$$h(\eta) = h(\lambda) = -h\lambda = -\lambda, \quad f(\blacklozenge) = \sqrt{\blacklozenge}, \quad g(\blacklozenge) = \sqrt{\blacklozenge}. \tag{13}$$

This choice is motivated by the following remarks.

(i) The yielding criterion here introduced coincides with delamination criteria which can be found in the literature [e.g. Brewer and Lagace (1988)].

(ii) Equations (13a, b, c) allow the interpretation of the plastic multiplier λ as a variable describing the degradation which varies in the interval [0, 1]. When λ reaches the value 1 ($\chi = -1$) the elastic domain is reduced to zero volume and the point can be considered completely damaged.

(iii) The nonassociativity, i.e. the choice $a_i' \neq b_i'$, $i = 1, 2, 3$, allows the independent introduction of different Fracture Energies G_{cI}, G_{cII}, G_{cIII}, as will be clear in Section 3 [eqn (44)].

(iv) A model similar to this one, but with associated flow rule, and a different interpretation of irreversible displacement discontinuities, has been used by Schellekens and de Borst (1991, 1992). The monodimensional version which takes into account the opening mode only (tractions in direction 3), has been used in Fracture Mechanics of concrete with the so called discrete crack models, for instance in Bažant and Oh (1983).

2.2. *Model b: elastic-damage*

Consider the special choice:

$$\Psi(\eta) \equiv 0, \quad G \equiv 0. \tag{14}$$

With the above choice the static and kinematic internal variables and the plastic displacement discontinuities reduce to zero. Hence an anisotropic elastic-damage model is obtained, in which the evolution of damage variables is nonassociated to damage function F. For the expression of damage function F and the evolution laws of damage variables d_i the following choice is made:

$$F = F(Y_i, \bar{Y}) = f(a_1'' Y_1 + a_2'' Y_2 + a_3'' Y_3) - \bar{Y} - 1, \tag{15}$$

$$\dot{d}_i = l_i(\bar{Y})\dot{\lambda} \quad i = 1, 2, 3, \quad \dot{\bar{Y}} = \dot{\lambda}. \tag{16}$$

In eqn (15) a_i'', $i = 1, 2, 3$ are non-negative model parameters; function f is positive, convex and differentiable; $f(0) = 0$. The elastic-damage model in point is therefore defined by relations (3) with $\Psi \equiv 0$, (4a, b), (8), (15) and (16). Notice that, due to eqns (15), (16) and the loading–unloading conditions (8), the evolution law for damage variables can be equivalently expressed as follows:

$$d_i = L_i(\bar{Y}) \equiv \int_0^{\bar{Y}} l_i(\bar{Y}')\,\mathrm{d}\bar{Y}' \quad i = 1, 2, 3, \quad \bar{Y} = \max\left\{1, \max_{\tau' \leqslant \tau}\left\{f\left(\sum_1^3 a_i'' Y_i(\tau')\right)\right\}\right\} - 1, \tag{17}$$

where τ is the current instant in time. The following restrictions determine the chosen damage evolution law:

$$L_i(0) = 0, \quad 0 \leqslant L_i(\bar{Y}) \leqslant 1, \quad \frac{\mathrm{d}L_i(\bar{Y})}{\mathrm{d}\bar{Y}} \geqslant 0 \quad i = 1, 2, 3, \tag{18}$$

$$d_3 = 1 \Rightarrow d_2 = d_1 = 1. \tag{19}$$

In view of the above equations (17) the evolution of the damage variables is governed by the choice of functions $L_i(\bar{Y})$ subjected to conditions (18). Relation (19) implies that when complete damage is reached for mode I (opening mode), also in modes II and III the interface is considered to be completely damaged.

Consider the mechanical dissipation ω per unit surface:

$$\omega = \sum_{1}^{3}{}_{i} t_i[\dot{u}_i] - \dot{E} = \sum_{1}^{3}{}_{i} Y_i \dot{d}_i. \tag{20}$$

The dissipation ω is never negative due to the expression of Y_i [eqn (4b)], the restrictions imposed on functions $L_i(\bar{Y})$ [eqn (18)] and the non-negativeness of $\dot{\lambda}$.

The model in point takes into account the anisotropy, the decrease in resistance and elastic stiffness, the unilateral effect. The three damage variables evolve at the same time, but the velocity of evolution can be independently governed by the choice of functions $L_i(\bar{Y})$. The quantity chosen to govern the damage criterion is a norm of energy variables associated to damage. The initial damage level is governed by parameters a_i'', $i = 1, 2, 3$.

A particular choice which will be used for further discussion and for numerical examples of Section 7 is the following:

$$f(\blacklozenge) = \sqrt{\blacklozenge}, \quad L_i(\bar{Y}) = \gamma_i'' \bar{Y} \quad i = 1, 2, 3. \tag{21}$$

In eqn (21b), γ_i'' are non-negative model parameters. The following remarks motivate the above choice:

(i) As for model a, the elastic domain in the space of tractions t_i coincides with delamination criteria in interlaminar stresses, frequently used in the literature. This can be seen by making use of eqns (4b) and the inverse of (4a) in order to substitute the variables Y_i in eqn (15).

(ii) A model similar to this one was recently used in the analysis of composite delamination by Allix (1989), Allix and Ladevèze (1992), Ladevèze (1992) and Daudeville (1992).

2.3. *Model c: elastic–plastic-damage*

Make the particular choices:

$$F = F(t_i, \chi; d_i) = G(t_i, \chi; d_i) = f(t_i; d_i) - \chi - 1, \tag{22a}$$

$$f(t_i; d_i) = f\left(a_1'''\left(\frac{t_1}{1-d_1}\right)^2 + a_2'''\left(\frac{t_2}{1-d_2}\right)^2 + a_3'''\left(\frac{\langle t_3\rangle_+}{1-d_3}\right)^2\right). \tag{22b}$$

Function f is subjected to the same restrictions as functions f for cases a and b; a_i''' are non-negative model parameters. With the above choices, the general model expressed by relations (2)–(8) reduces to an elastic–plastic-damage model for interface with evolution of plastic displacement discontinuities and kinematic internal variables both associated to the yielding-damage function F. In the present case function $\Psi(\eta)$ which governs the hardening is supposed to be convex of variable η which, in turn, coincides with λ in view of eqns (6b) and (22a). The evolution of damage variables is still assumed not associated and is specified by the following relations:

$$\dot{d}_i = l_i(\chi)\dot{\lambda} = l_i^*(\chi)\dot{\chi} \quad i = 1, 2, 3. \tag{23}$$

By taking into account eqns (22), (23) and (8), the evolution law for damage variables can be equivalently expressed as follows:

$$d_i = L_i(\chi) \equiv \int_0^{\chi} l_i^*(\chi')\,\mathrm{d}\chi' \quad i = 1, 2, 3, \quad \chi = \max\left\{1, \max_{\tau' \leqslant \tau}\{f(t_i(\tau'); d_i(\tau'))\}\right\} - 1. \tag{24}$$

The above expression for the evolution of damage variables coincides formally with eqns (17) if one identifies variable χ with $\bar{Y}$. Restrictions (18) and (19) also hold in this case.

Consider the mechanical dissipation ω per unit surface:

$$\omega = \sum_{1}^{3} t_i[\dot{u}_i] - \dot{E} = \sum_{1}^{3} t_i[\dot{u}_i^{\mathrm{p}}] - \chi\dot{\eta} + \sum_{1}^{3} Y_i\dot{d}_i \geqslant (f(t_i; d_i) - \chi)\dot{\lambda} + \sum_{1}^{3} Y_i\dot{d}_i. \tag{25}$$

Inequality (25c) has been obtained by taking into account the evolution equations (6a, b), by considering the expression (22) of $F = G$, and by making use of the convexity and differentiability of f with respect to t_i and of the fact that $f(0) = 0$. The non-negativeness of ω follows from relations (25c), (22a), (8a, b, c) and from the non-negativeness of the dissipation term due to damage.

The following particular choice is considered for further discussion and numerical examples of Section 7:

$$h(\eta) = h(\lambda) = h\lambda, \quad f(\blacklozenge) = \sqrt{\blacklozenge}, \quad L_i(\chi) = 1 - \sqrt{1 - 2\gamma_i'''\chi} \quad i = 1, 2, 3, \tag{26}$$

where γ_i''' are non-negative model parameters.

The particular evolution law for damage variables given by eqns (24) and (26d) is such that a critical state is reached for $d_i = 1$ with zero tractions and a finite value of displacement discontinuities $[u_i]_c$. This fact is not in general guaranteed for arbitrary choices of functions $L_i(\chi)$. For instance choice (21b) made for model b (with $\bar{Y}$ substituted by χ) would imply infinite displacement discontinuities for $d_i = 1$.

2.4. *Remarks*

(i) The main differences between the classes of models a, b and c can be remarked for cyclic loading. In that case, in fact, irreversible displacement discontinuities and stiffness degradation play a crucial role. It appears that the more adequate model in these situations is one of kind c.

(ii) The three classes of models introduced, with the special choices made for the shape of the elastic domain and for the evolution laws of damage variables, can be formally represented with a unique set of equations, in which variables have to be adequately interpreted depending on the model chosen. The set of equations is given by eqns (2), (8) and the following:

$$t_i = (1 - d_i)K_i[u_i]^{\mathrm{e}} \quad i = 1, 2, \quad t_3 = (1 - d_3)K_3^{+}\langle[u_3]^{\mathrm{e}}\rangle_{+} + K_3^{-}\langle[u_3]^{\mathrm{e}}\rangle_{-}, \tag{27}$$

$$Y_i = \tfrac{1}{2}K_i[u_i]^{\mathrm{e}2} \quad i = 1, 2, \quad Y_3 = \tfrac{1}{2}K_3^{+}\langle[u_3]^{\mathrm{e}}\rangle_{+}^2, \tag{28}$$

$$Y_{\mathrm{a}} \equiv a_1\left(\frac{t_1}{1 - d_1}\right)^2 + a_2\left(\frac{t_2}{1 - d_2}\right)^2 + a_3\left(\frac{\langle t_3\rangle_{+}}{1 - d_3}\right)^2, \tag{29a}$$

$$Y_{\mathrm{b}} \equiv b_1\left(\frac{t_1}{1 - d_1}\right)^2 + b_2\left(\frac{t_2}{1 - d_2}\right)^2 + b_3\left(\frac{\langle t_3\rangle_{+}}{1 - d_3}\right)^2, \tag{29b}$$

$$F = \sqrt{Y_a} + a_4\frac{t_3}{(1 - d_3)} - \chi - 1 = \sqrt{Y_a} + a_4\frac{t_3}{(1 - d_3)} - h(\lambda) - 1, \tag{30}$$

$$[\dot{u}_i]^{\mathrm{p}} = \frac{b_i}{(1 - d_i)^2}\frac{t_i}{\sqrt{Y_b}}\dot{\lambda} \quad i = 1, 2, \quad [\dot{u}_3]^{\mathrm{p}} = \frac{b_3}{(1 - d_3)^2}\frac{\langle t_3\rangle_{+}}{\sqrt{Y_b}}\dot{\lambda}, \tag{31}$$

$$d_i = L_i(\chi) = L_i(h(\lambda)) \quad i = 1, 2, 3. \tag{32}$$

Scalar variables Y_a and Y_b are defined in eqns (29) for notation convenience. Classes of models a, b, c are obtained from the above equations by setting respectively:

model a: $L_i(\chi) \equiv 0, \quad a_i = a'_1, \quad b_i = b'_1 \quad i = 1,2,3, \quad h(\lambda) = -\lambda;$

model b: $b_i = 0, \quad a_i = \dfrac{a''_i}{2K_i} \quad i = 1,2,3, \quad a_4 = 0, \quad h(\lambda) = \lambda, \quad L_i(\chi) = \gamma''_i \chi \quad i = 1,2,3,$

model c: $a_i = b_i = a''_i \quad i = 1,2,3, \quad a_4 = 0, \quad L_i(\chi) = 1 - \sqrt{1 - 2\gamma'''_i \chi} \quad i = 1,2,3.$

3. DECOHESION PROCESSES AND INTERFACE MODELS

The interface models introduced in Section 2 have as their main common characteristic the fact that they simulate the process of decohesion between two solids, in particular in the case of delamination in laminated composites. Mainly to the purpose of model identification, it is important to analyse some energetic aspects of a decohesion process as described by an interface model.

Consider an infinitesimal element of surface $d\Gamma$ centred on point P (Fig. 1). A *decohesion process* (DP) is here defined as a history of displacement discontinuities $[\mathbf{u}]$ in point P which lead to a complete decohesion of surface $d\Gamma$ between the two solids in contact, i.e. to complete separation. Given an interface constitutive law and a DP, the work necessary to separate the two solids is computed by:

$$w_d \, d\Gamma = \left(\int_{DP} \sum_1^3 t_i \, d[u_i] \right) d\Gamma. \tag{33}$$

In eqn (33) w_d is the work of decohesion per unit surface; in general w_d is a function of the material, i.e. of the interface model, and of the DP followed.

Three particular DPs are chosen to characterize the loss of cohesion of two solids. These three processes result by imposing an increasing displacement discontinuity of the same sign only in directions 1, 2, 3 respectively (modes II, III, I). The resulting values of w_d will be called w_{dII}, w_{dIII}, w_{dI}:

$$w_{dI} = \int_{DP_I} t_3 \, d[u_3], \quad w_{dII} = \int_{DP_{II}} t_1 \, d[u_1], \quad w_{dIII} = \int_{DP_{III}} t_2 \, d[u_2]. \tag{34}$$

For the particular choices made for interface models a, b, c of Section 2, the DP in uniaxial situations always ends when a finite critical level $[u_i]_c$ of displacement discontinuities is reached. Moreover, integrals in eqns (34) do not change if elastic unloading and reloading are performed during the uniaxial DP. w_{dI}, w_{dII}, w_{dIII} can therefore be rewritten as:

$$w_{dI} = \int_0^{[u_3]_c} t_3 \, d[u_3], \quad w_{dII} = \int_0^{[u_1]_c} t_1 \, d[u_1], \quad w_{dIII} = \int_0^{[u_2]_c} t_2 \, d[u_2]. \tag{35}$$

From eqns (35) it follows that the work of decohesion per unit surface w_d in uniaxial situations is represented by the areas under the uniaxial curves $t_i - [u_i]$ (Fig. 2). For mixed-modes I, II, III, it is in general not possible to derive energetic quantities w_d expressed in terms of w_{dI}, w_{dII}, w_{dIII}.

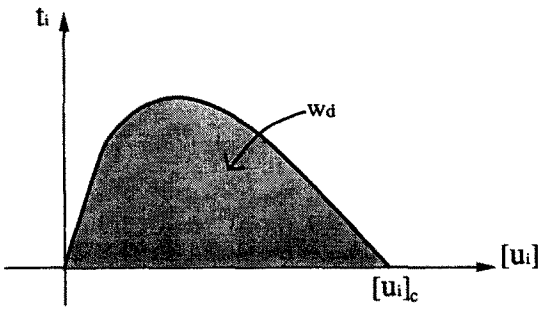

Fig. 2. Uniaxial response and work of decohesion per unit surface.

Consider now a phenomenon of loss of cohesion which involves a finite surface Γ. The work W_d necessary to separate the two solids is in this case equal to:

$$W_d = \int_\Gamma w_d \, d\Gamma = \int_\Gamma \int_{DP} \left(\sum_1^3 t_i \, d[u_i] \right) d\Gamma. \tag{36}$$

In general W_d depends on the material (the interface model) and the DPs which are generally different at every point of the surface Γ. W_d depends therefore on the distribution of displacement discontinuities [**u**] on Γ. If at every point of the surface Γ the DP is the same, the work W_d can be expressed as:

$$W_d = w_d \Gamma = \left(\int_{DP} \sum_1^3 t_i \, d[u_i] \right) \Gamma. \tag{37}$$

In the above very particular case it is therefore possible to directly correlate the energy of a process of loss of cohesion that involves a finite surface to a quantity depending only on the interface model and a specific DP. In order to identify the parameters of an interface model by measure of energetic quantities, one should obtain tests verifying the above situation. In particular if the DP in every point of the surface Γ coincides with one of the simple processes defined previously (modes I, II, III) the work W_d is given by:

$$W_{dI} = w_{dI} \Gamma, \quad W_{dII} = w_{dII} \Gamma, \quad W_{dIII} = w_{dIII} \Gamma. \tag{38}$$

Fracture Mechanics tests may be used to identify the interface models. To this purpose the fracture test must satisfy two main conditions. First the process zone at the crack tip, in which the majority of damage phenomena are concentrated, must translate without modifying its shape, i.e. a steady-state situation for crack propagation must be attained; in this case in fact all the points belonging at some instant to the process zone will undergo the same DP. Second the process zone must be such that its schematization as a surface at crack tip is reasonable (Fig. 3). If this is true the interface model can be used to describe the process zone. In this kind of fracture test the measured energy per unit surface necessary to propagate a crack of a finite length (finite because it is measured in real tests), i.e. the *Critical Energy Release Rate* G_c, can then be directly correlated to W_d:

$$G_c = \frac{W_d}{\Gamma} = \int_{DP} \sum_1^3 t_i \, d[u_i] \tag{39}$$

and therefore directly correlated to the interface model. In particular if the crack propagates in pure modes I, II or III, one can write:

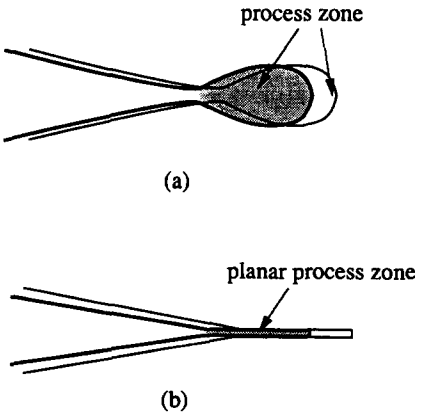

Fig. 3. (a) Process zone at crack tip. (b) Planar schematization for the process zone.

$$G_{cI} = w_{dI}, \quad G_{cII} = w_{dII}, \quad G_{cIII} = w_{dIII}. \tag{40}$$

3.1. *Remarks*

(i) As already mentioned, relations (39) and (40) hold if the fracturing process is such that the process zone translates without modification (steady-state fracture propagation) and the damage phenomena of the process zone are concentrated on a surface at the crack tip. The first hypothesis corresponds to situations in which the diagram of the Energy Release Rate G versus the crack length [*fracture resistance curve*, Broek (1989)] reaches a stationary value, i.e. G does not vary with crack length. The second hypothesis is not unusual in Fracture Mechanics, in fact it is implicitely assumed when fracture propagation is modelled through the use of interface models [see e.g. Bažant and Oh (1983)].

(ii) By considering the established connection between the Critical Energy Release Rate G_c and the energy necessary for a decohesion process [eqns (36) and (39)], it is seen that in general G_c cannot be simply expressed, for coupled modes, as a simple function of parameters G_{cI}, G_{cII}, G_{cIII}; G_c also depends on the DP, i.e. on the path followed in the space of displacement discontinuities. It also appears that in general G_c will depend both on material and the distribution of DP in the process zone [eqn (36)]. Hence, in the framework of the present schematization, G_c cannot in general be simply interpreted as a material parameter.

(iii) In the case of linear elastic Fracture Mechanics, the process zone can be thought of as reduced to a point at the crack tip. Hence the Critical Energy Release Rate is rigorously a material parameter for a given process of fracture.

4. IDENTIFICATION OF INTERFACE MODELS FOR THE ANALYSIS OF COMPOSITE DELAMINATION

One of the major drawbacks for the use of interface models in the analysis of composite delamination is the difficulty in identifying model parameters.

In the literature a number of delamination tests have been proposed [see e.g. Donaldson (1988), Pagano (1989) and Suo *et al.* (1992)], the most popular are perhaps the double cantilever beam (DCB), the end notch flexure (ENF) and the split cantilever beam (SCB) tests, for delamination in modes I, II and III respectively (Fig. 4). In these tests the hypotheses of remark (i) in Section 3 are reasonably satisfied, other tests proposed (Suo *et al.*, 1992) can probably more exactly satisfy the conditions but are still not largely used. Due to the popularity of DCB, ENF and SCB tests, they will be taken here as a reference to compute parameters G_{cI}, G_{cII} and G_{cIII}. It is worth noticing that parameters G_{cI}, G_{cII}, G_{cIII} are always derived by making some hypotheses on the global behaviour of the specimen used in the test. Generally a hypothesis of global elastic behaviour for fixed crack length is made; for instance in the DCB test when use is made of the compliance method to compute G_{cI}. Besides the three crucial parameters G_{cI}, G_{cII} and G_{cIII}, other information could be used in order to identify interface models, as will be suggested in Section 4.1.

It is worth noting that the choice of interface elastic stiffnesses K_i does not appear to be crucial for delamination analysis. These parameters can be chosen by applying the method used in Lene (1986), Allix (1989) and Daudeville (1992) where the interface is interpreted as an equivalent homogeneous layer with very small thickness. The elastic stiffness parameters are in this case given by:

$$K_1 \cong \frac{2G_{13}}{e}, \quad K_2 \cong \frac{2G_{23}}{e}, \quad K_1^+ \cong \frac{E_3}{e}. \tag{41}$$

In eqns (41) e is the fictitious thickness attributed to the interface, e.g. a fraction of layer thickness; G_{13}, G_{23} and E_3 are shear and Young moduli and can be chosen equal to the same parameters of a layer of the laminated composite supposed homogeneous.

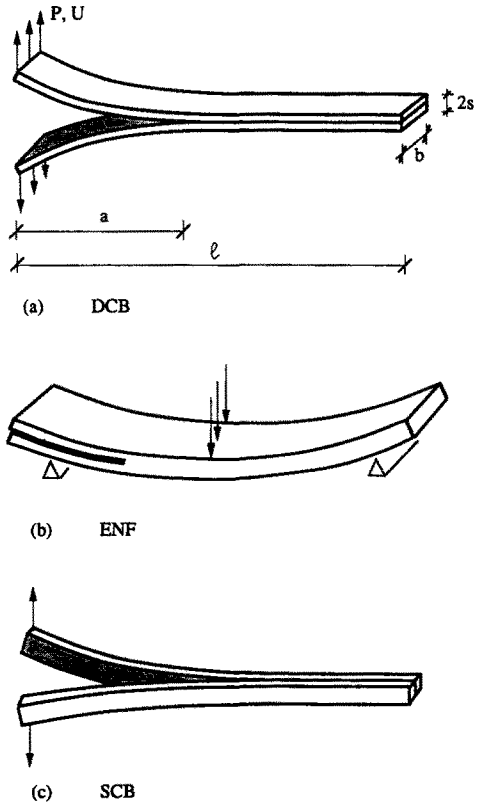

Fig. 4. Delamination test specimens. (a) Mode I: Double Cantilever Beam. (b) Mode II: End Notched Flexure. (c) Mode III: Split Cantilever Beam.

4.1. *Identification of three particular interface models*

For the models a, b and c presented in Section 2, an identification procedure is now proposed. For the three cases treated, the elastic parameters K_i are supposed to be chosen as suggested above. The special choices (13), (21) and (26) are assumed, hence reference can be made to the set of equations (2), (8) and (27)–(32) with specializations regarding each model.

(a) *Elastic–plastic-softening model.* For identification purposes it is useful to study the uniaxial behaviour. In the particular case treated here and with the further specialization of $a_4 = 0$ the monodimensional behaviour under monotonically increasing displacement discontinuity is given by the following relations for $i = 1, 2, 3$:

$$t_i = K_i[u_i] \qquad \text{if } 0 \leqslant [u_i] \leqslant \frac{1}{K_i\sqrt{a_i}}, \tag{42a}$$

$$t_i = \left(\frac{1}{K_i} - \frac{\sqrt{a_i b_i}}{h}\right)^{-1}\left([u_i] - \frac{\sqrt{b_i}}{h}\right) \quad \text{if } \frac{1}{K_i\sqrt{a_i}} \leqslant [u_i] \leqslant \frac{\sqrt{b_i}}{h} = [u_i]_c, \tag{42b}$$

where no summation on repeated indices is implied. Recall that parameter h is assumed to be equal to unity [eqn (13c)].

The identification of parameters a_i and b_i of the model can be made as described below.

—Yielding function parameters a_i.

The values of tensile strength t_{30} and shear strengths t_{10}, t_{20} of the homogenized layer or of the matrix can be used to impose the maximum on the uniaxial response in terms of tractions, thus obtaining:

$$a_i = \frac{1}{t_{i0}^2} \quad i = 1, 2, 3. \tag{43}$$

—Plastic potential parameters b_i.
Relations (35) and (40) can be used. The integral in eqns (35) can in this case be easily computed being the monodimensional behaviour given by a bilinear law. It is straightforward to obtain:

$$G_{cII} = \frac{1}{2h}\sqrt{\frac{b_1}{a_1}}, \quad G_{cIII} = \frac{1}{2h}\sqrt{\frac{b_2}{a_2}}, \quad G_{cI} = \frac{1}{2h}\sqrt{\frac{b_3}{a_3}}. \tag{44}$$

(b) *Elastic–damage model.* Consider again the monodimensional behaviour under monotonically increasing displacement discontinuity. By exploiting the relations of the model in the uniaxial case for $i = 1, 2, 3$, one still obtains in the elastic range eqn (42a), while for the nonlinear damage range:

$$t_i = (1+\gamma_i - \gamma_i K_i\sqrt{a_i}[u_i])K_i[u_i] \quad \text{if } \frac{1}{K_i\sqrt{a_i}} \leqslant [u_i] \leqslant \frac{1+\gamma_i}{\gamma_i K_i\sqrt{a_i}} = [u_i]_c, \tag{45}$$

where superscript $''$ on γ_i has been dropped for simplicity.

Note that for $\gamma_i > 1$ the maximum of the uniaxial curve corresponds to the elastic limit, while for $\gamma_i < 1$ the maximum is reached in the post-elastic range. The identification of parameters a_i and γ_i can be made as suggested below:

—Damage function parameters a_i.
The value of tractions corresponding to the end of linear range could be chosen equal to t_{0i} by making use of eqn (43). t_{0i} could be obtained e.g. by acoustic emission measurements.

—Damage evolution parameters γ_i.
Relations (35) and (40) can be used. The computation of integrals in eqn (35) gives:

$$G_{cII} = \frac{1+3\gamma_1+3\gamma_1^2}{6K_1 a_1 \gamma_1^2}, \quad G_{cIII} = \frac{1+3\gamma_2+3\gamma_2^2}{6K_2 a_2 \gamma_2^2}, \quad G_{cI} = \frac{1+3\gamma_3+3\gamma_3^2}{6K_3^+ a_3 \gamma_3^2}. \tag{46}$$

Relations (46) can be used to compute γ_i once the values of Critical Energy Release Rates are known and values of K_i and a_i are fixed. The inversion of eqns (46) in terms of γ_i gives rise to a second order equation which has in general a negative root not to be considered.

(c) *Elastic–plastic-damage model.* As in the preceding examples consider first the uniaxial behaviour under monotonically increasing displacement discontinuity. By reducing the equations of the model to the uniaxial case, the following parametric form of the relation between traction and displacement discontinuity in the nonlinear range can be obtained for $i = 1, 2, 3$ (superscript $'''$ on γ_i dropped for simplicity):

$$t_i = \sqrt{1-2\gamma_i\chi}(\chi+1)\frac{1}{\sqrt{a_i}}, \quad [u_i] = \frac{\chi+1}{K\sqrt{a_i}} + \frac{\sqrt{a_i}}{\gamma_i h}(1-\sqrt{1-2\gamma_i\chi})$$

$$\text{if } \frac{1}{K_i\sqrt{a_i}} \leqslant [u_i] \leqslant \frac{2\gamma_i h + h + 2K_i a_i}{2\gamma_i h K_i\sqrt{a_i}} = [u_i]_c, \quad 0 \leqslant \chi \leqslant \frac{1}{2\gamma_i} = \chi_c. \tag{47}$$

In the elastic range eqn (42a) still holds. Notice that when $h = 1$, for $\gamma_i > 1$ the maximum of the uniaxial curve corresponds to the elastic limit, while for $\gamma_i < 1$ the maximum is reached in the post-elastic range. A possible identification procedure for parameters a_i, h and γ_i is suggested below:

—Parameters a_i.
They can be identified as done in example *b*.

—Parameter h.
This parameter, which governs the hardening behaviour, should in principle be derived from information concerning the plastic response of the interface. Since this information is not available, one can use information concerning the plastic response of the matrix idealizing the interface as a small thickness layer made of the same material used for the matrix. For simplicity in the following of this paper it will be assumed $h = 1$.

—Parameters γ_i.
As in examples a and b relations (35) and (40) can be used. The integral in eqn (35) can be computed by making use of parametric relations (42a) and (47), it results in:

$$w_i = \frac{1}{K_i a_i}\left(\frac{1}{2} + \frac{1}{15\gamma_i^2} + \frac{1}{3\gamma_i}\right) + \frac{1}{8\gamma_i^2 h} + \frac{1}{2\gamma_i h}, \tag{48a}$$

$$G_{\mathrm{cII}} = w_1, \quad G_{\mathrm{cIII}} = w_2, \quad G_{\mathrm{cI}} = w_3. \tag{48b, c, d}$$

Relations (48) can be used to compute γ_i once K_i, a_i and h are fixed. One obtains a second order equation in γ_i, the positive root is the correct one.

5. NUMERICAL INTEGRATION OF INTERFACE MODELS

As is usual in structural analyses and necessary in the presence of consitutive softening, the integration of the interface law here presented is kinematically driven. Being the situation in terms of all static and kinematic variables known at a certain time instant τ_n, and given a finite increment of displacement discontinuities $\Delta[\mathbf{u}] \equiv [\mathbf{u}]_{n+1} - [\mathbf{u}]_n$ between the time instant τ_n and τ_{n+1}, all other variables are found at time instant τ_{n+1} through the numerical integration scheme. Here and in the following a subscript n or $n+1$ means a quantity computed at time instant τ_n or τ_{n+1} respectively, the symbol $\Delta(\blacklozenge)$ means an increment in the quantity $\blacklozenge$ in a time interval $[\tau_n, \tau_{n+1}]$.

5.1. *Backward difference integration*

The *backward difference* integration rule is adopted here; this is an implicit scheme which belongs to the category of return mapping algorithms and is commonly used in nonlinear computational mechanics [see e.g. Perego (1988) and Comi *et al.* (1991)].

The numerically integrated version of eqns (2), (8), (27)–(32) reads:

$$[\mathbf{u}]_{n+1} = [\mathbf{u}]_n + \Delta[\mathbf{u}] = [\mathbf{u}]^{\mathrm{e}}_{n+1} + [\mathbf{u}]^{\mathrm{p}}_{n+1}, \tag{49}$$

$$t_{i_{n+1}} = (1 - d_{i_{n+1}}) K_i [u_i]^{\mathrm{e}}_{n+1} \quad i = 1, 2, \tag{50a}$$

$$t_{3_{n+1}} = (1 - d_{3_{n+1}}) K_3^+ \langle [u_3]^{\mathrm{e}}_{n+1} \rangle_+ + K_3^- \langle [u_3]^{\mathrm{e}}_{n+1} \rangle_-, \tag{50b}$$

$$Y_{i_{n+1}} = \tfrac{1}{2} K_i [u_i]^{\mathrm{e}^2}_{n+1} \quad i = 1, 2, \quad Y_{3_{n+1}} = \tfrac{1}{2} K_3^+ \langle [u_3]^{\mathrm{e}}_{n+1} \rangle_+^2, \tag{51}$$

$$\chi_{n+1} = \left.\frac{\mathrm{d}\Psi}{\mathrm{d}\eta}\right|_{n+1} \equiv h(\eta_{n+1}) = h(\lambda_{n+1}), \tag{52}$$

$$F_{n+1} = \sqrt{Y_{a_{n+1}}} + a_4 \frac{t_{3_{n+1}}}{(1 - d_{3_{n+1}})} - h(\lambda_{n+1}) - 1, \tag{53}$$

$$\Delta[u_i]^{\mathrm{p}} = \frac{b_i}{(1 - d_{i_{n+1}})^2} \frac{t_{i_{n+1}}}{\sqrt{Y_{b_{n+1}}}} \Delta\lambda \quad i = 1, 2, \quad \Delta[u_3]^{\mathrm{p}} = \frac{b_3}{(1 - d_{3_{n+1}})^2} \frac{\langle t_{3_{n+1}} \rangle_+}{\sqrt{Y_{b_{n+1}}}} \Delta\lambda, \tag{54}$$

$$d_{i_{n+1}} = L_i(\chi_{n+1}) = L_i(h(\lambda_{n+1})), \tag{55}$$

$$F_{n+1} \leqslant 0, \quad F_{n+1}\Delta\lambda = 0, \quad \Delta\lambda \geqslant 0. \tag{56}$$

The above relations (49)–(56), together with restrictions introduced in Section 2 on functions L_i represent a nonlinear constitutive law which relates the displacement discontinuities $[\mathbf{u}]_{n+1}$ to tractions $\mathbf{t}_{n+1}$.

Given an increment of displacement discontinuities $\Delta[\mathbf{u}]$ and all quantities at τ_n being known, the solution is found through an *elastic prediction* phase, a *check of consistency* and a *plastic–damage corrector* phase, following the typical scheme of a return mapping algorithm:

(1) Elastic predictor (elastic trial response).
A purely elastic response to $[\mathbf{u}]_{n+1} = [\mathbf{u}]_n + \Delta[\mathbf{u}]$ is first computed by considering fixed values at τ_n the variables λ, $[u_i]^p$ and d_i. This phase consists of simple function evaluations.

(2) Check of consistency.
The plastic-damage condition is checked on the basis of the elastic trial response. If F_{n+1}^{trial} is less than or equal to zero, then the response in the step is purely elastic and the solution at τ_{n+1} is given by the elastic trial response; the process stops. If F_{n+1}^{trial} is greater than zero, the response is plastic-damage and a plastic-damage corrector phase is necessary; the process continues from phase 3.

(3) Plastic-damage corrector.
The process is plastic-damage, hence the solution will give a positive plastic multiplier increment $\Delta\lambda$. The system of nonlinear equations (49)–(56) must be satisfied with $F_{n+1} = 0$ due to eqns (56) and the fact that $\Delta\lambda$ is strictly positive. This phase consists therefore of solving the nonlinear system of equations (49)–(55) and (56a) with an equality sign ($F_{n+1} = 0$).

The solution of this nonlinear system could be found by using one of the existing numerical strategies. In the Appendix A.1 a solution scheme which decouples the plastic and the damage part of the constitutive law is proposed and detailed for the case of positive $t_{3_{n+1}}$. This scheme has been used for the solution of numerical examples of Section 7.

Remarks

(i) For constitutive models of class b presented in Section 2 (elastic-damage) the damage corrector phase is straightforward. It can be performed by first computing χ_{n+1} from the consistency condition, recalling that in this case $a_4 = 0$:

$$\chi_{n+1} = \sqrt{Y_{a_{n+1}}} - 1 \tag{57}$$

and then obtaining the values of $d_{i_{n+1}}$ and $t_{i_{n+1}}$ from eqns (55) and (50). In eqn (57) $Y_{a_{n+1}}$ is computed starting from values of $Y_{i_{n+1}}$ given by eqns (51), in which $[\mathbf{u}]^e_{n+1} = [\mathbf{u}]_{n+1}$ is the input quantity for the step.

(ii) Particular care should be taken for situations corresponding to critical level of damage, i.e. when the displacement discontinuities $[\mathbf{u}]$ are near to the critical value $[\mathbf{u}]_c$. After the critical situation is reached, the interface is supposed to be completely damaged, i.e. the adjacent layers in the case of composites are separated. Only the behaviour in compression gives tractions different from zero (unilateral effect).

5.2. *Consistent tangent matrix*

A numerical scheme proposed for the integration of a constitutive law is likely to be accompanied by the computation of the *consistent tangent operator* (Simo and Taylor, 1985). The use of the consistent tangent operator is important in nonlinear analyses when, for the solution of global equilibrium, the equilibrium equation is linearized; as an example consider the Newton–Raphson method for a step-by-step analysis.

In the present context the consistent tangent operator is the Jacobian of the relation between tractions and displacement discontinuities, at time instant τ_{n+1}, as defined by the numerical integration scheme adopted:

$$\delta \mathbf{t} = \mathbf{J}\delta[\mathbf{u}]. \tag{58}$$

In eqn (58) $\mathbf{J}$ is the consistent tangent 3×3 matrix; $\mathbf{J}$ has to be computed from the system of equations (49)–(56) by taking the derivatives of each equation and by distinguishing the cases of elastic unloading and plastic-damage loading. The unilateral effect introduced in the model also obliges to distinguish cases with positive or negative tractions in direction 3. In Appendix A2 the case with positive $t_{3_{n+1}}$ is detailed.

6. AN ALGORITHM FOR THE SOLUTION OF A BOUNDARY VALUE PROBLEM IN THE PRESENCE OF SOFTENING INTERFACES

6.1. *Boundary value problem*

Consider an elastic body defined by the domain Ω which contains a certain number n of internal surfaces Γ_j of discontinuity. Each surface is characterized by an interfacial constitutive law of the kind described in Section 2. The body is submitted to body forces $\mathbf{f}$ in Ω and to surface loading $\mathbf{F}$ on the part $\partial_F\Omega$ of its external surface; kinematic constraints $\mathbf{u} = \mathbf{u}_0$ are imposed on $\partial_u\Omega$ (see Fig. 5). Small strain and displacement theory, isothermal conditions, no inertia effects will be assumed.

The problem of delamination in composites can be treated with the above schematization. The single fibre-reinforced layers can be conceived as purely elastic (the domain Ω) and connected by nonlinear interfaces (the *discontinuity surfaces* Γ_j). If the body Ω is supposed to behave nonlinearly (e.g. with a plastic-damage constitutive law), the damage phenomenon can also involve the layers and thus permit a more realistic idealization.

Define Γ' as the union of all surfaces Γ_j and $\Omega' \equiv \Omega - \Gamma'$. The class of displacement vectors $\mathbf{u}^*$ which are zero on $\partial_u\Omega$ and *regular* in Ω' (virtual displacements) is named U; notice that $\mathbf{u}^*$ (and the real displacements) can be discontinuous on Γ'.

The boundary value problem in point consists of finding the fields of displacements $\mathbf{u}$ and stresses $\boldsymbol{\sigma}$ which satisfy the following relations:

(1) Compatibility.

$\mathbf{u}$ is *regular* in Ω' and $\mathbf{u} = \mathbf{u}_0$ on $\partial_u\Omega$.

(2) Equilibrium.

for any $\mathbf{u}^* \in U$:

$$\int_{\Omega'} \boldsymbol{\sigma}^{\mathrm{T}}\boldsymbol{\varepsilon}(\mathbf{u}^*)\,\mathrm{d}\Omega + \int_{\Gamma'} \mathbf{t}^{\mathrm{T}}[\mathbf{u}^*]\,\mathrm{d}\Gamma = \int_{\Omega'} \mathbf{f}^{\mathrm{T}}\mathbf{u}^*\,\mathrm{d}\Omega + \int_{\partial_F\Omega} \mathbf{F}^{\mathrm{T}}\mathbf{u}^*\,\mathrm{d}\Sigma. \tag{59}$$

(3) Constitutive law.

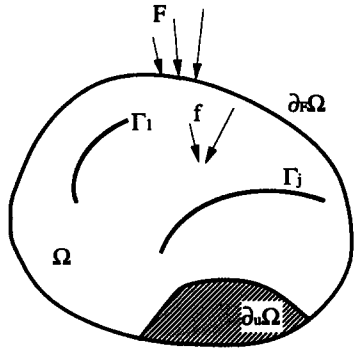

Fig. 5. A continuum Ω with discontinuity interfaces Γ_j.

$$\boldsymbol{\sigma} = \mathbf{E}\boldsymbol{\varepsilon}(\mathbf{u}) \quad \text{in } \Omega', \quad \mathbf{t} = A([\mathbf{u}], \mathbf{x}) \quad \text{on } \Gamma'. \tag{60}$$

In eqn (59) $\boldsymbol{\sigma}$ is a vector which gathers the six independent components of the symmetric Cauchy stress tensor; $\boldsymbol{\varepsilon}(\mathbf{u})$ is a six component vector of strains related to the displacement field $\mathbf{u}$ through the linear differential relations of small strain theory; $\boldsymbol{\sigma}$ and $\boldsymbol{\varepsilon}$ are defined in such a way that the scalar product $\boldsymbol{\sigma}^{\mathrm{T}}\boldsymbol{\varepsilon}$ equals the scalar product of stress and strain tensors. Recall that the vector $\mathbf{t}$ in eqn (59) is the vector of tractions on surfaces Γ_j, the sign conventions are the same as defined at the beginning of Section 2 (Fig. 1). Relation (60a) is the Hooke law for the elastic body, $\mathbf{E}$ is a 6×6 matrix of elastic moduli; eqn (60b) has the same meaning of eqn (1).

The nonlinear (due to the interfacial constitutive law) boundary value problem (59)–(60) can be discretized in space by using the compatible finite element (FE) method. The application of the FE method is straightforward, the only nonstandard difficulty is represented by the second integral in eqn (59), i.e. by the presence of discontinuity surfaces Γ_j. This difficulty can be overcome with the introduction of *interfacial finite elements* as already done in the recent literature in particular for composite delamination problems. With an interface finite element the interpolation of the displacement discontinuity vector $[\mathbf{u}]$ on a generic surface Γ_j is directly derived from the interpolation used for the displacement field $\mathbf{u}$ in the adjacent finite elements (see Fig. 6):

$$[\mathbf{u}] = \mathbf{u}^+ - \mathbf{u}^- = \boldsymbol{\Phi}^+\mathbf{U}^+ - \boldsymbol{\Phi}^-\mathbf{U}^- \equiv \mathbf{B}^{\mathrm{int}}\mathbf{U}^{\mathrm{int}}. \tag{61}$$

In the above equation $\mathbf{U}^+$ and $\mathbf{U}^-$ are the nodal degrees of freedom for nodes which belong to Ω_+ and Ω_- respectively and are on surface Γ (Fig. 6); $\boldsymbol{\Phi}^+$ and $\boldsymbol{\Phi}^-$ are interpolation function matrices. By introducing the above interpolations in eqn (59), the following equilibrium equation is obtained:

$$\mathbf{K}_E\mathbf{U} + \sum_{\Gamma_k}^{n_{\mathrm{int}}} \mathbf{H}_k^{\mathrm{int}} \int_{\Gamma_k} \mathbf{B}_k^{\mathrm{int}^{\mathrm{T}}} \mathbf{t}_k^{\mathrm{T}} \, \mathrm{d}\Gamma = \mu\mathbf{P}. \tag{62}$$

In eqn (62) $\mathbf{K}_E$ is the assembled elastic stiffness matrix for the domain Ω; $\mathbf{U}$ is the vector of global degrees of freedom; $\mathbf{H}_k^{\mathrm{int}}$ are Boolean matrices which formally represent the assemblage for each interfacial element k ($\mathbf{U}_k^{\mathrm{int}} = \mathbf{H}_k^{\mathrm{int}}\mathbf{U}$); $\mathbf{P}$ is the vector of equivalent nodal loads and μ is a load parameter. The second term in eqn (62) is the internal force vector deriving from the *cohesive interfaces* Γ_j.

6.2. *An algorithm with local control*

The particular difficulties which can be encountered in the numerical solution of boundary value problems in the presence of softening had already been envisaged in the literature at the end of the sixties (Maier, 1968), in particular snap-through and snap-back behaviours can be found. This kind of global behaviour can be tackled by making use of special algorithms, originally proposed for elastic stability problems, among them *in primis*

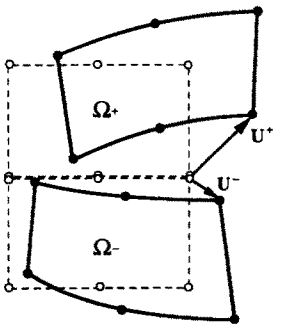

Fig. 6. Finite elements neighbouring a discontinuity interface.

those of Riks (1972), Wempner (1971), Crisfield (1981) and Ramm (1981) [see also Crisfield and Shi (1992) as a review article]. The common idea which characterizes the majority of these algorithms is that to derive the analysis through an additional condition implying the control of a quantity which in general is neither a loading parameter nor a displacement. The choice of an alternative driving quantity can be in general achieved by treating the loading parameter as a variable in the equilibrium equation and by adding an equation often called the *constraint relationship*. The constraint can be of a global kind, as in the *arc-length* method (Crisfield, 1981) or of a local one as proposed by de Borst (1987). Chen and Schreyer (1990) recently proposed to locally control the analysis for softening continua through a total strain norm in a suitably chosen point.

In the analysis of composite delamination, algorithms of the above kind, with local control, have recently been used. In the present paper an algorithm is proposed in which the controlled quantity is a total displacement discontinuity norm in a certain point of an interface. As an example, this procedure applied to composite delamination in pure mode I situations reduces to control the opening displacements of the delamination fracture. The resulting method generalizes the preceding ones used for composite delamination and can be applied to the analysis of mixed-mode situations and to the analysis of situations in which more than one delamination fracture propagates.

The response of the elastic body containing a certain number of interfaces is to be computed in a time interval $[0, T]$. By choosing convenient instants $0 = \tau_0, \tau_1, \tau_2, \ldots, \tau_n$ the time interval is subdivided in time steps $\Delta\tau = \tau_{n+1} - \tau_n$. Being the response known at a time instant τ_n, eqn (62) is solved at time instant τ_{n+1}:

$$\mathbf{q}(\mathbf{U}_{n+1}) - \mu_{n+1}\mathbf{P} = 0, \quad \mathbf{q}(\mathbf{U}_{n+1}) \equiv \mathbf{K}_E\mathbf{U}_{n+1} + \sum_{1}^{n_{\text{int}}} \mathbf{H}_k^{\text{int}} \int_{\Gamma_k'} \mathbf{B}_k^{\text{int}^{\mathrm{T}}} \mathbf{t}_{k_{n+1}}^{\mathrm{T}} \, d\Gamma. \tag{63}$$

In eqns (63) $\mathbf{q}(\mathbf{U}_{n+1})$ can be considered as a known nonlinear function of variables $\mathbf{U}_{n+1}$. The dependence of $\mathbf{q}$ on $\mathbf{U}_{n+1}$ is given by eqn (63b), by the finite element interpolation of interfacial elements and by the numerically integrated interface constitutive law. As seen in Section 5 the numerical integration procedure for the interface model gives in fact the values of traction $\mathbf{t}_{n+1}$ at a time instant τ_{n+1} with the situation at τ_n being known and the total displacement discontinuity $[\mathbf{u}]_{n+1}$, i.e. the vector $\mathbf{U}_{n+1}$ being known. In eqn (63a), $\mathbf{U}_{n+1}$ and μ_{n+1} are both considered as variables. Equation (63a) is then to be solved together with a scalar constraint relationship. The constraint relationship is derived from the local control of the displacement discontinuity in a suitably chosen point R of an interface Γ_j. The chosen point R for the step $[\tau_n, \tau_{n+1}]$ is that with the greater value of the multiplier λ (a measure of the degree of degradation for all the models of Section 2) at instant τ_n among the Gauss points of interface elements which are not already completely damaged. The variable controlled is a norm of the displacement discontinuity increment $\Delta[\mathbf{u}]^R = [\mathbf{u}]_{n+1}^R - [\mathbf{u}]_n^R$ in the point R:

$$\mathbf{c}^{\mathrm{T}}\Delta[\mathbf{u}]^R = \alpha. \tag{64}$$

In the above equation α is a fixed parameter, $\mathbf{c}$ is a 3-components vector of weighting coefficients. Vector $\mathbf{c}$ governs the kind of imposed fracturing process, e.g. for $\mathbf{c}^{\mathrm{T}} = (0, 0, 1)$ a pure mode I opening situation will be imposed. The choice of $\mathbf{c}$ can be automatically made in the algorithm by considering the results obtained at the end of the last step:

$$\mathbf{c} = \frac{[\mathbf{u}]_n^R}{\|[\mathbf{u}]_n^R\|}, \quad \|[\mathbf{u}]\| = \sqrt{[u_1]^2 + [u_2]^2 + [u_3]^2}. \tag{65}$$

The constraint (64) can be expressed in terms of the vector $\mathbf{U}_{n+1}$ by making use of eqn (61) and the definition of matrix $\mathbf{H}^{\text{int}}$ in eqn (62), hence the computations for each step consist of the solution of the following equations in the unknowns $\mathbf{U}_{n+1}$ and μ_{n+1}:

$$\mathbf{q}(\mathbf{U}_{n+1}) - \mu_{n+1}\mathbf{P} = 0, \quad \mathbf{c}^{\mathrm{T}}\Delta[\mathbf{u}]^{R} - \alpha \equiv \mathbf{c}^{\mathrm{T}}\mathbf{B}^{*}(\mathbf{U}_{n+1} - \mathbf{U}_{n}) - \alpha = 0. \tag{66}$$

In eqn (66b) matrix $\mathbf{B}^{*}$ has been defined as: $\mathbf{B}^{*} = \mathbf{B}^{\mathrm{int}\,R}\mathbf{H}^{\mathrm{int}\,R}$. The nonlinear system (66) is solved iteratively by applying a method of the Newton–Raphson kind. Notice that eqn (66b) is linear in the unknown $\mathbf{U}_{n+1}$, therefore only a linearization of eqn (66a) is necessary.

The algorithm proposed above has been applied for the solution of numerical examples for composite delamination problems presented in Section 7. Some details on the iterative procedure for the solution of system (66) are given in Appendix A.3.

7. NUMERICAL EXAMPLES

In this section some numerical examples will be presented, they are mainly conceived to:

(1) show the potentiality of the class of interface constitutive models introduced in Section 2;

(2) clarify the identification procedure proposed with the discussion of Sections 3 and 4;

(3) verify the validity of the numerical integration algorithm described in Section 5 for the interface constitutive law;

(4) illustrate the behaviour of the algorithm proposed in Section 6.2 for the solution of the boundary value problem of Section 6.1;

(5) apply all the procedures envisaged to the analysis of composite delamination and verify the validity of the idealization adopted.

To discuss points (1) and (3) above, the three example models a, b, c of Section 2 are considered. For values of parameters which give in the three cases the same Critical Energy Release Rate in modes I, II, III and the same elastic interface stiffnesses, the different models are numerically integrated under different histories of displacement discontinuities in pure modes and mixed modes. For the three models the values of interface stiffnesses K_i, of parameters a_i and of Critical Energy Release Rates are the following:

$$K_1 = K_2 = K_3^{+} = K_3^{-} = 100\,000\ \mathrm{N\,mm^{-3}},$$
$$a_1 = a_2 = a_3 = 0.4 \times 10^{-3}\ \mathrm{mm^4\,N^{-1}},$$
$$G_{\mathrm{cII}} = G_{\mathrm{cIII}} = 0.8\ \mathrm{N\,mm^{-1}}, \quad G_{\mathrm{cI}} = 0.4\ \mathrm{N\,mm^{-1}}.$$

The other parameters are different for each model and are given below:

—Model a elastic–plastic-softening.

$$b_1 = b_2 = 1.024 \times 10^{-3}\ \mathrm{mm^4\,N^{-2}}, \quad b_3 = 0.256 \times 10^{-3}\ \mathrm{mm^4\,N^{-2}},$$
$$a_4 = 0\ \mathrm{mm^2\,N^{-1}}, \quad h = 1\ \mathrm{mm\,N^{-1}},$$
$$[u_1]_{\mathrm{c}} = [u_2]_{\mathrm{c}} = 0.032\ \mathrm{mm}, \quad [u_3]_{\mathrm{c}} = 0.016\ \mathrm{mm}.$$

Parameters b_i have been computed by applying eqn (44).

—Model b elastic-damage.

$$\gamma_1 = \gamma_2 = 0.08111, \quad \gamma_3 = 0.12107,$$
$$[u_1]_{\mathrm{c}} = [u_2]_{\mathrm{c}} = 0.0067\ \mathrm{mm}, \quad [u_3]_{\mathrm{c}} = 0.0046\ \mathrm{mm}.$$

Parameters γ_i have been computed by applying eqn (46).

—Model c elastic–plastic-damage.

$$\gamma_1 = \gamma_2 = 0.83755, \quad \gamma_3 = 1.52603, \quad h = 1 \text{ mm N}^{-1},$$
$$[u_1]_c = [u_2]_c = 0.0249 \text{ mm}, \quad [u_3]_c = 0.0139 \text{ mm}.$$

Equations (48) relate the values of G_{cI}, G_{cII}, G_{cIII} to model parameters.

In Figs 7–9 are compared the results of numerical integration of the three models for different histories of displacement discontinuities. Figure 7 collects the responses for pure mode I (displacement discontinuities in direction 3 only). Figure 7(a) shows the applied displacement discontinuity history corresponding to responses of models a and c reported in Figs 7(b) and 7(c), respectively. In Figs 7(d, e) are reported the history of applied displacement discontinuity and the corresponding interface response for model b. The histories of loading have been chosen different for models a, c and b in order to better show the qualitative behaviour of the interface models in all the three cases. In Figs 7(b, c, e) the unilateral effect is to be remarked, i.e. for negative tractions t_3 (compression on the interface) the behaviour is always unlimitedly elastic and the stiffness remains unchanged. The presence of irreversible displacement discontinuities can be observed in Figs 7(b, c), while the

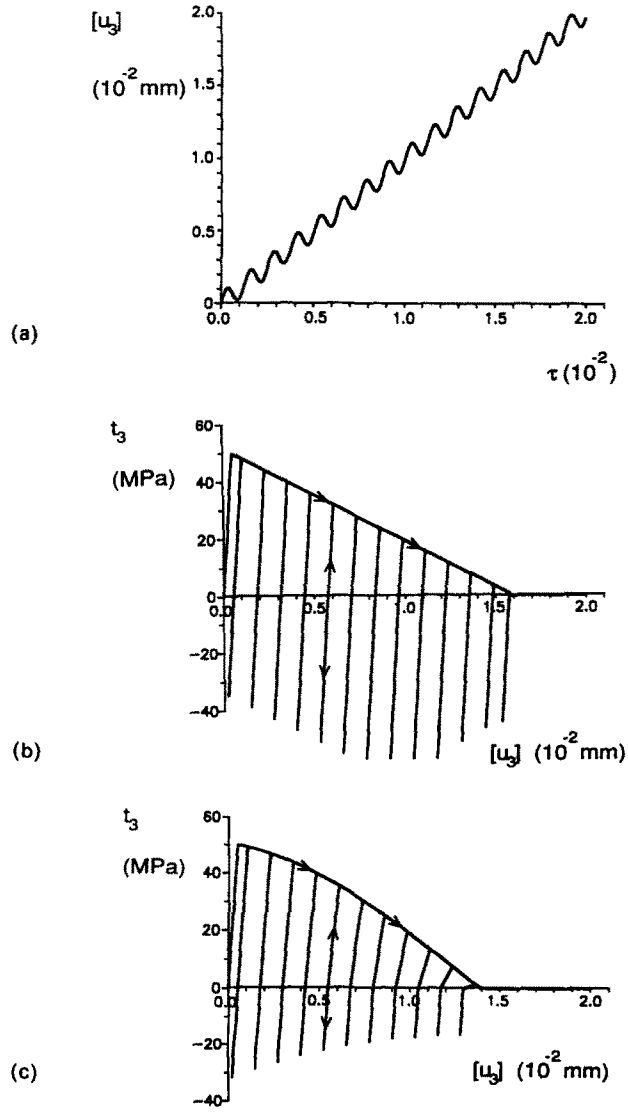

Fig. 7. Results of the numerical integration of interface models for pure mode-I loading. (a) Displacement discontinuity history for models a and c. (b) Model a, elastic–plastic-softening, response. (c) Model c, elastic–plastic-damage, response. (d) Displacement discontinuity history for model b. (e) Model b, elastic-damage, response. (*Continued overleaf.*)

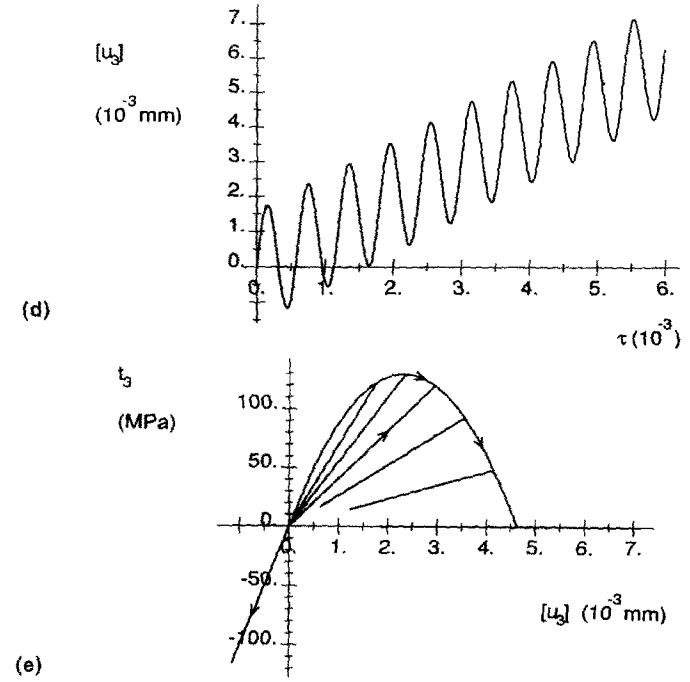

Fig. 7 (*continued*).

degradation of elastic stiffness in Figs 7(c, e). Notice the coupled effect of stiffness degradation and irreversible displacement discontinuities in Fig. 7(c), i.e. for model c the unloading is elastic with an elastic stiffness which changes while the damage process goes on and irreversible displacement discontinuities are present. The behaviours in pure mode II (displacement discontinuities in direction 1 only) are compared in Fig. 8. The applied displacement discontinuity history is shown in Fig. 8(a), while the corresponding responses for models a, b and c are reported in Figs 8(b, c, d) respectively. Examples of responses in mixed-mode situations are shown in Fig. 9. The history of displacement discontinuity of Fig. 9(a) is applied to the three directions $i = 1, 2, 3$, in order to obtain the mixed-mode responses for the three models reported with a dashed line in Figs 9(b, c, d). For the three cases a direct comparison is possible with the responses obtained in pure-mode (solid line) obtained by applying the history of Fig. 9(a) in direction 3 only. In all three cases it can be observed that the effect of coupled modes accelerates the damage, i.e. the critical value of displacement discontinuity for which the traction is zero is diminished in the case of mixed modes.

Points 2, 4 and 5 at the beginning of Section 7 are now discussed with reference to the numerical simulation of a specimen with the shape of a DCB [Fig. 4(a)] under pure mode I or mixed modes loading conditions. The finite element model of the DCB consists of two rows of beam elements connected through interfacial elements (Fig. 10); note that in Fig. 10 the nonzero thickness is introduced only for graphical convenience, the coordinates of nodes for upper and lower beams coincide. For the beam elements plane strain conditions and displacements fields of Timoshenko type have been used. The nodal degrees of freedom for beam elements are the displacements U_1 in the direction parallel to the beam axis, U_3 in the direction perpendicular to the beam axis, the rotation θ and the first derivative U'_3 of displacement U_3. These degrees of freedom are relative to the mid-plane of the specimen, i.e. to the inferior part of the upper beam and the superior one of the lower beam. This particular assumption for the kinematic description of the specimen allows an easier introduction of interface elements. The interfacial elements connect the adjacent nodes of the two rows of beam elements; the nodal degrees of freedom for interface are U_3, U'_3 and U_1. The beam elements are linear elastic, while to the interfacial elements a constitutive law of the kind of Section 2 is attributed. One end of the structure is built in, on the other extreme a load is applied as shown in Fig. 10. The spatial integrals are computed by means

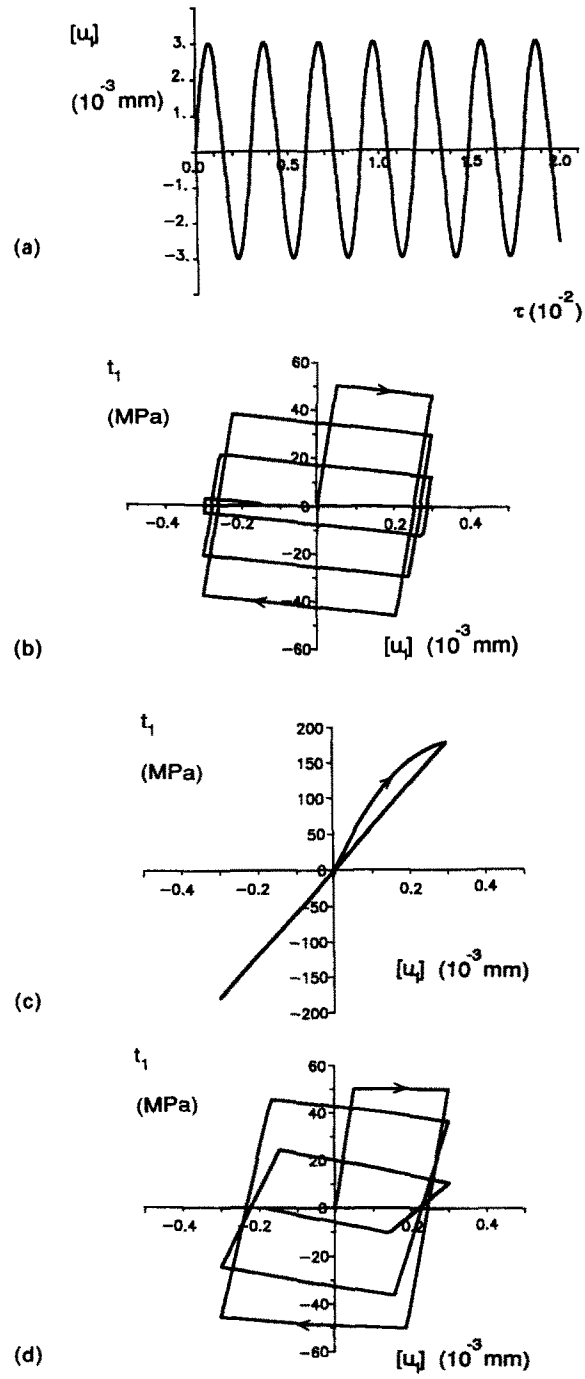

Fig. 8. Results of the numerical integration of interface models for pure mode-II loading. (a) Displacement discontinuity history for models a, b and c. (b) Model a, elastic–plastic-softening, response. (c) Model b, elastic-damage, response. (d) Model c, elastic–plastic-damage, response.

of a Gaussian quadrature rule. Three Gauss points are considered for each element. In order to apply the algorithm described in Section 6 the displacement discontinuity vector at each Gauss point is computed starting from eqn (61), in which $\mathbf{\Phi}^+$ and $\mathbf{\Phi}^-$ are interpolation functions used for upper and lower beam elements, and $\mathbf{U}^+$ and $\mathbf{U}^-$ are nodal degrees of freedom used for the interface in the upper and lower beam nodes respectively.

The geometrical data for the first case treated are:

$$a = 3 \text{ mm}, \quad b = 1 \text{ mm}, \quad s = 1 \text{ mm}, \quad l = 20 \text{ mm}, \quad \beta = \pi/2,$$

where a, b, s and l have the meaning of Fig. 4(a), angle β is defined in Fig. 10. The initial

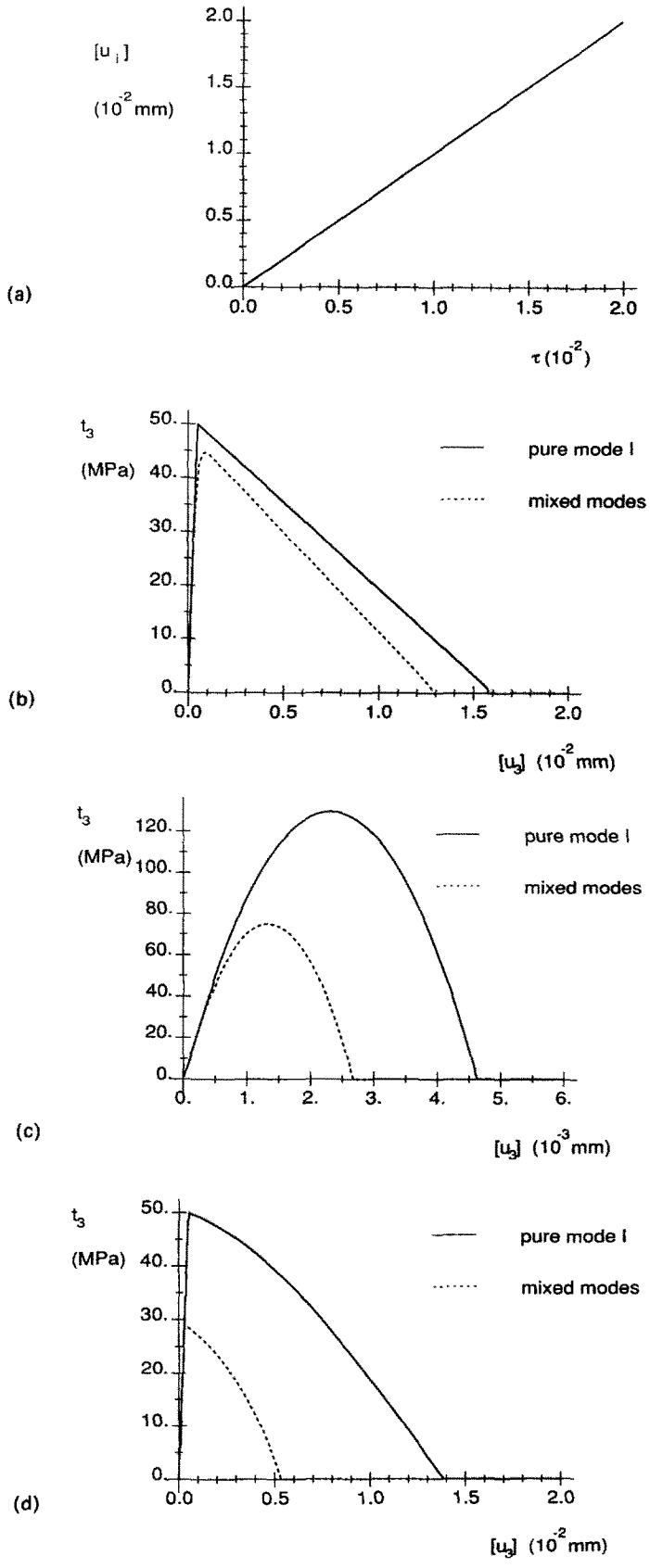

Fig. 9. Results of the numerical integration of interface models for mode-I and mixed-modes loading. (a) Displacement discontinuity history for models a, b and c. (b) Model a, elastic–plastic-softening, response. (c) Model b, elastic-damage, response. (d) Model c, elastic–plastic-damage, response.

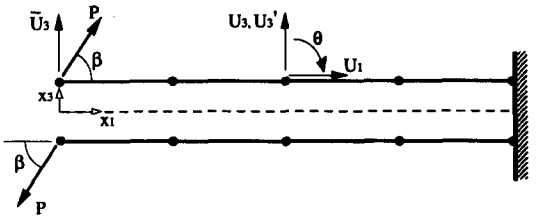

Fig. 10. Finite element scheme for the DCB examples.

fissure is introduced by giving the interface elements which are involved an elastic behaviour for compression in direction 3 and no cohesion at all for tension in direction 3 and for shear. Due to the loading conditions and geometry of the example, the numerical analysis simulates a pure mode I DCB test. The progression of the fissure results to be controlled by the increment of displacement discontinuities in direction 3 imposed at each step in the Gauss point nearest to the crack tip. This Gauss point in fact results to be the one with the highest value of multiplier λ (the most degradated one) among the Gauss points not already completely damaged. The analyses for this example are made with a mesh which divides the length of the DCB in 200 elements of decreasing size from the crack tip to the built in end. The smallest element has a length of 0.05 mm. This allows to well compute the tractions at the crack tip in the first phase of crack propagation. The three interfacial models a, b, c, defined by the previously given parameters are considered in the analyses (recall that $G_{cII} = G_{cIII} = 0.8$ N mm^{-1}; $G_{cI} = 0.4$ N mm^{-1}). The beam elements are considered elastic with parameters:

$$E_{11} = 135\,000 \text{ MPa}, \quad G_{13} = 5700 \text{ MPa},$$

where E_{11} is the Young modulus in direction 1 and G_{13} is the shear modulus for shear in the plane 1–3. The above data coincide with those of an homogeneized elementary ply of a T300/914 fibre composite. Each beam can therefore be considered as composed of a lay up of ten 0.1 mm thickness layers with fibers all directed in direction 1, i.e. a 0°/0° DCB test is simulated. The algorithm of Section 6 is applied for the analyses [matrix **Q** equal to the consistent tangent matrix evaluated at each iteration. *cf.* Appendix (A3)]; the parameter α is in general taken as equal to about one half of the critical displacement discontinuity $[\mathbf{u}]_c$ for the interfacial model chosen.

In Figs 11–13 the results are represented of the analyses made with model b. Figure (11) represents the distribution of tractions in direction 3 at crack tip for an elastic situation [Fig. 11(a)] and its evolution until crack propagation [Fig. 11(b)]. The evolution is represented by 13 subsequent curves relative to distributions of tractions at the crack tip; the 12th curve shows that the stresses at the crack tip are zero and therefore crack propagation starts. In Fig. 12(a) the diagram of load at the extremum of the beam versus the vertical displacement at the same point is reported; Fig. 12(b) shows the same diagram for the first steps of the analysis. Figure 12(c) shows the diagram of the compliance $C = \bar{U}_3/P$ versus fissure length computed during the numerical analysis. The comparison between Figs 11(b) and 12(b) shows that in the treated example the fissure starts to propagate when the maximum load level is reached (the 12th circle on the curve, apart from that on the origin, which correspond to the 12th curve in Fig. 11(b)]. The influence of spatial discretization can be judged from Fig. 13(a) where the load–displacement diagrams obtained for different meshes are compared. The meshes differ for the dimension of the smallest elements. Figure 13(b) shows the influence of parameter α on the global response.

In Fig. 14 two responses obtained by making use of model a with the previously given parameters are shown, in order to evaluate the influence on the global response of the interface stiffness K. The load–displacement curves for these two cases are shown in Fig. 14(a), in Fig. 14(b) are represented the uniaxial responses for the corresponding interface models. The case with higher stiffness results in a more ductile behaviour for the interface which is reflected in the global nonlinear behaviour shown in Fig. 14(a). It is to be noted

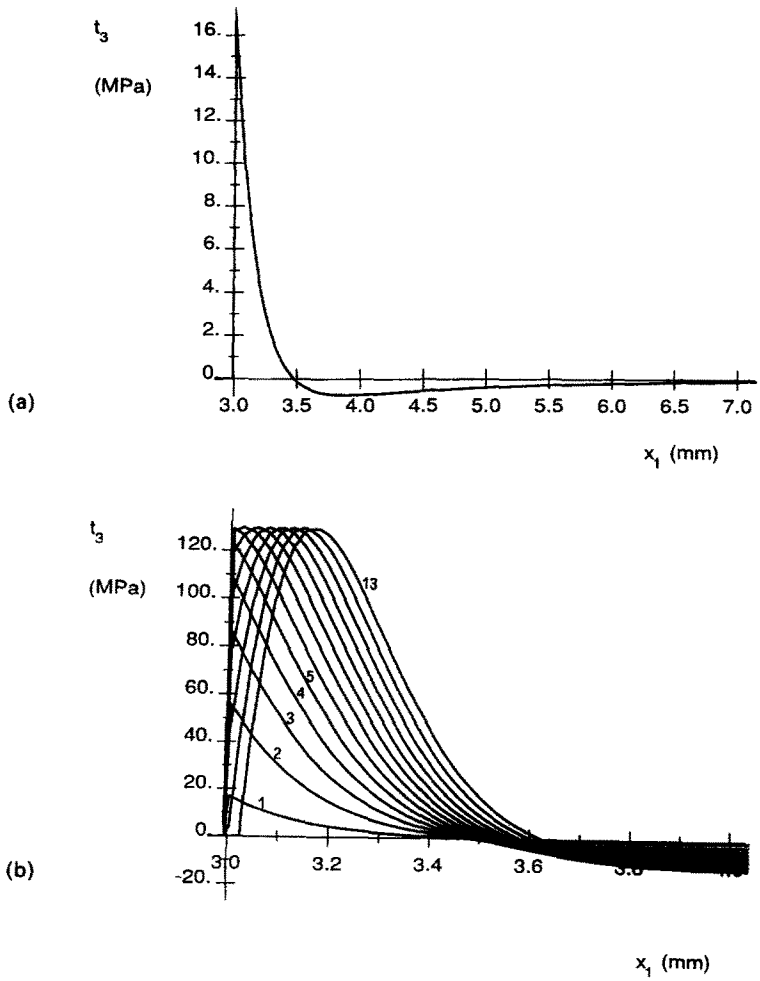

Fig. 11. Example 1, elastic-damage interface model; normal stress at crack tip. (a) Elastic situation with load $P = 1N$. (b) Evolution of normal stress at crack tip until crack propagation.

that the maximum of the P–U curve and the decreasing part (propagation range) do not differ at all in the two cases. Since the interface stiffness depends on the fictitious thickness e attributed to the interface [eqn (41)], it can be concluded that the value of e doesn't have a great influence on the global response of the specimen and on the initiation of propagation.

A comparison of results obtainable with different interface models is shown in Fig. 15. In Fig. 15(a) the uniaxial responses in direction 3 of the three interfacial models used are compared. In Fig. 15(b) a comparison of the global response obtained with the three models is illustrated. Notice that the responses differ negligibly, a remarkable difference can be observed only around the maximum load value for model b, this is due to the high value of the maximum on the diagram $t_3 - [u_3]$ [Fig. 15(a)] for model b. The fact that the curves do not differ considerably is due to the choice of interface model parameters which give the same Critical Energy Release Rate in mode I. As already remarked in Sections 3 and 4, this is really the crucial parameter which has to be introduced in the interface models. In the chosen example the monotonically progressing fracturing process doesn't greatly distinguish among different interface models if they furnish the same Critical Energy Release Rate; moreover in this case a model which doesn't take into account the behaviour during unloading would have given the same results. In Fig. 15(c) the differences in global response for the three models can be appreciated from the unloading paths. These are obtained by making, during the numerical analysis, some steps with negative values of parameter α.

The second case treated is that of a DCB specimen with the same geometrical data as the above one, but subjected to a mixed mode loading. The interface model b has been used in the analysis ($G_{cII} = G_{cIII} = 0.8$ N mm^{-1}; $G_{cI} = 0.4$ N mm^{-1}), with parameters previously

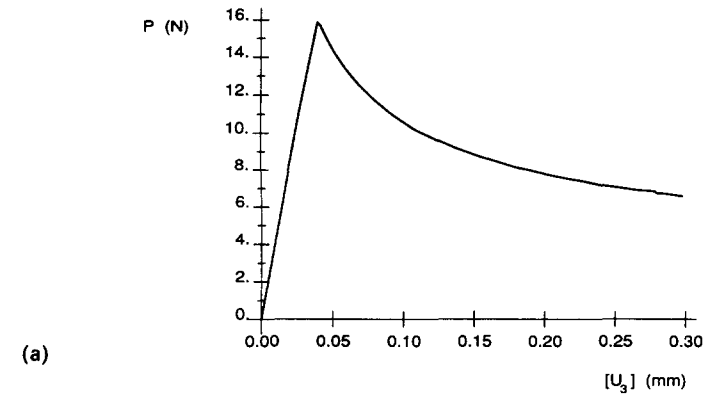

(a)

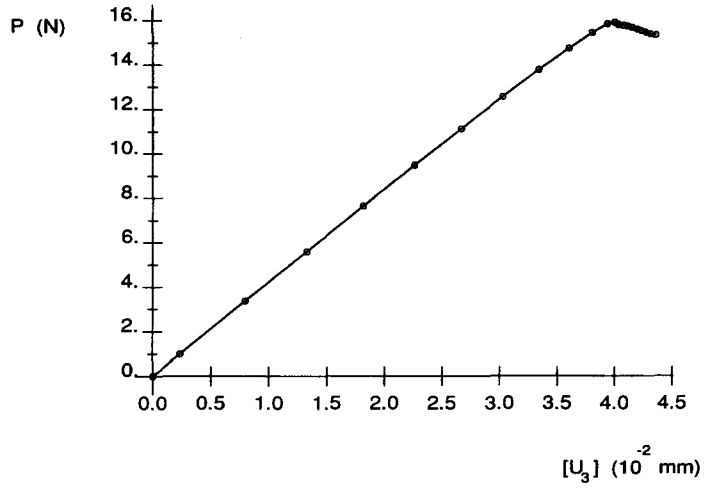

(b)

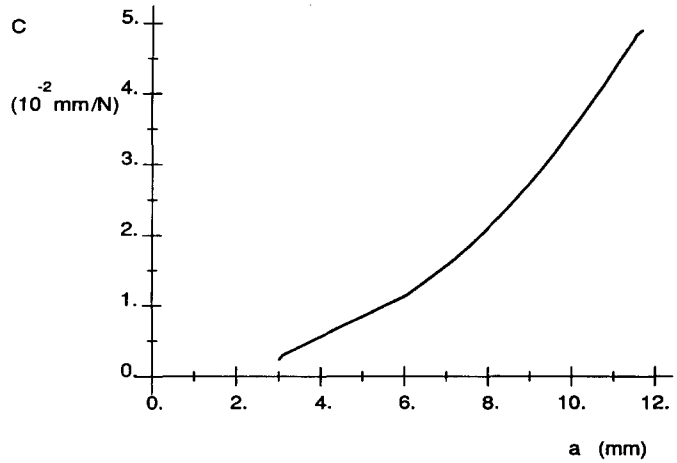

(c)

Fig. 12. Example 1, elastic-damage interface model. (a) Load versus displacement. (b) Load versus displacement for the first 21 steps. (c) Compliance versus fissure length.

defined. The load is obtained with a value of angle β in Fig. 10 equal to $\pi/4$. In Fig. 16(a) are shown the diagrams of displacement discontinuities in directions 1 and 3 (shear and opening modes) versus the coordinate x_1 when the fissure is already propagated at about 1.5 mm. The distribution of interfacial stresses t_1 and t_3 at the same instant is represented in Fig. 16(b). In Fig. 16(c) the diagram of load component in direction 3 versus the

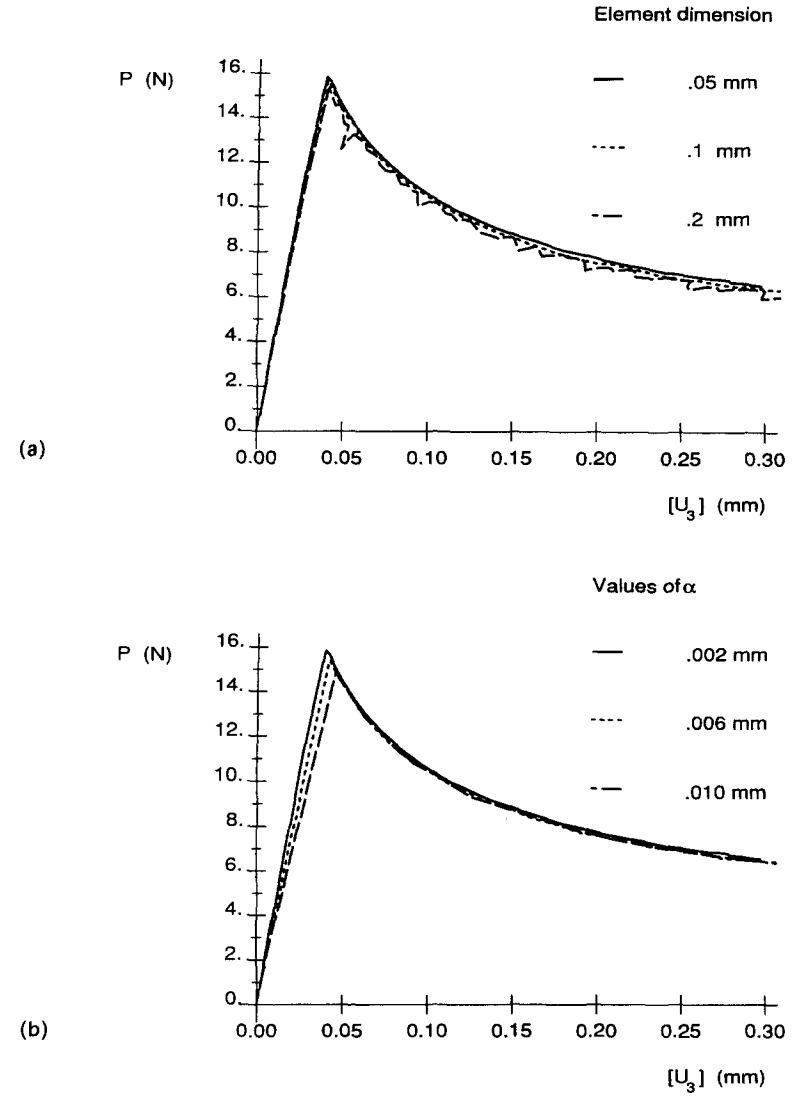

Fig. 13. Example 1, elastic-damage interface model. (a) Influence of spatial discretization on load versus displacement response. (b) Influence of control parameter α on load versus displacement response.

nodal displacement component in the same direction is represented. Figure (16) shows the capability of the algorithm to follow situations of mixed mode propagation.

The third case treated is that of a DCB test ($\beta = \pi/2$), with geometric dimensions usually adopted in real tests, which have been taken from Ye (1992). In this reference a $0°/0°$ lay up of T300/934 DDS carbon fiber was tested. The geometrical data, the elastic parameters of homogeneized layers and the Critical Energy Release Rate calculated from the experiment are reported here below:

$$a = 30 \text{ mm}, \quad b = 2.5 \text{ mm}, \quad s = 6.25 \text{ mm}, \quad l = 230 \text{ mm},$$
$$E_{11} = 133\,000 \text{ Mpa}, \quad G_{13} = 4200 \text{ Mpa}, \quad E_{33} = 7700 \text{ Mpa},$$
$$G_{cI} = 0.643 \text{ N mm}^{-1}.$$

The numerical analysis is done with the purpose of comparing the global response with the experimental one reported in Ye (1992). The procedure adopted to define the parameters for the analyses, made with interface models a and b, can be schematized in the following

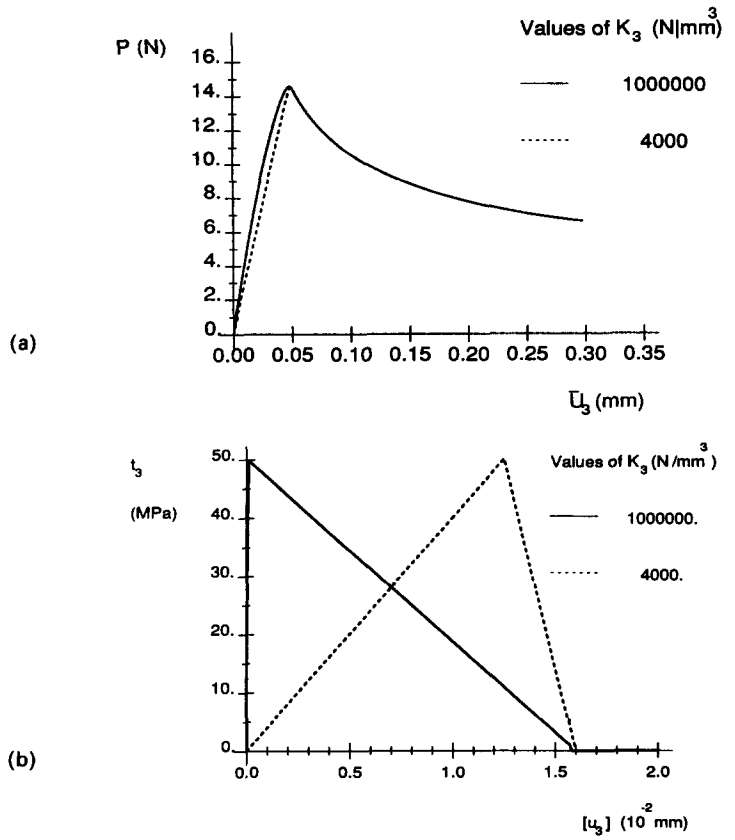

Fig. 14. Example 1, elastic–plastic-softening interface model. (a) Influence of interface stiffness on load versus displacement response. (b) Uniaxial responses of the interface model.

steps:

(1) An identification is made for the shear elastic stiffness parameters used for beam elements in order to obtain the global elastic stiffness of the DCB specimen.

(2) The elastic stiffness parameter K_3 for the interface is computed by applying eqn (41c) with E_{33} given above and e equal to 0.026 mm (about one fifth of a single layer thickness).

(3) A tensile strength t_{30} equal to 60 Mpa is supposed for the interface. This parameter is used to identify parameter a_3 for both models a elastic–plastic-softening and b elastic damage used in the analysis, by use of formula (43).

(4) For model a the parameter b_3 is identified by making use of eqn (44c) with $h = 1$ and G_{Ic} given above. For model b parameter γ_3 is identified by applying eqn (46c) with the same value for G_{Ic}.

(5) The dimension of the smallest finite elements used for the spatial discretization of the beam is taken to be equal to 0.05 mm.

Notice that, being the analysis in pure mode I, only parameters with index 3 are necessary. The resulting values used in the numerical computations for models a and b are reported below:

—for both models a and b

$$K_3^+ = K_3^- = 300\,000 \text{ N mm}^{-3},$$
$$a_3 = 0.278 \times 10^{-3} \text{ mm}^4 \text{ N}^{-2};$$

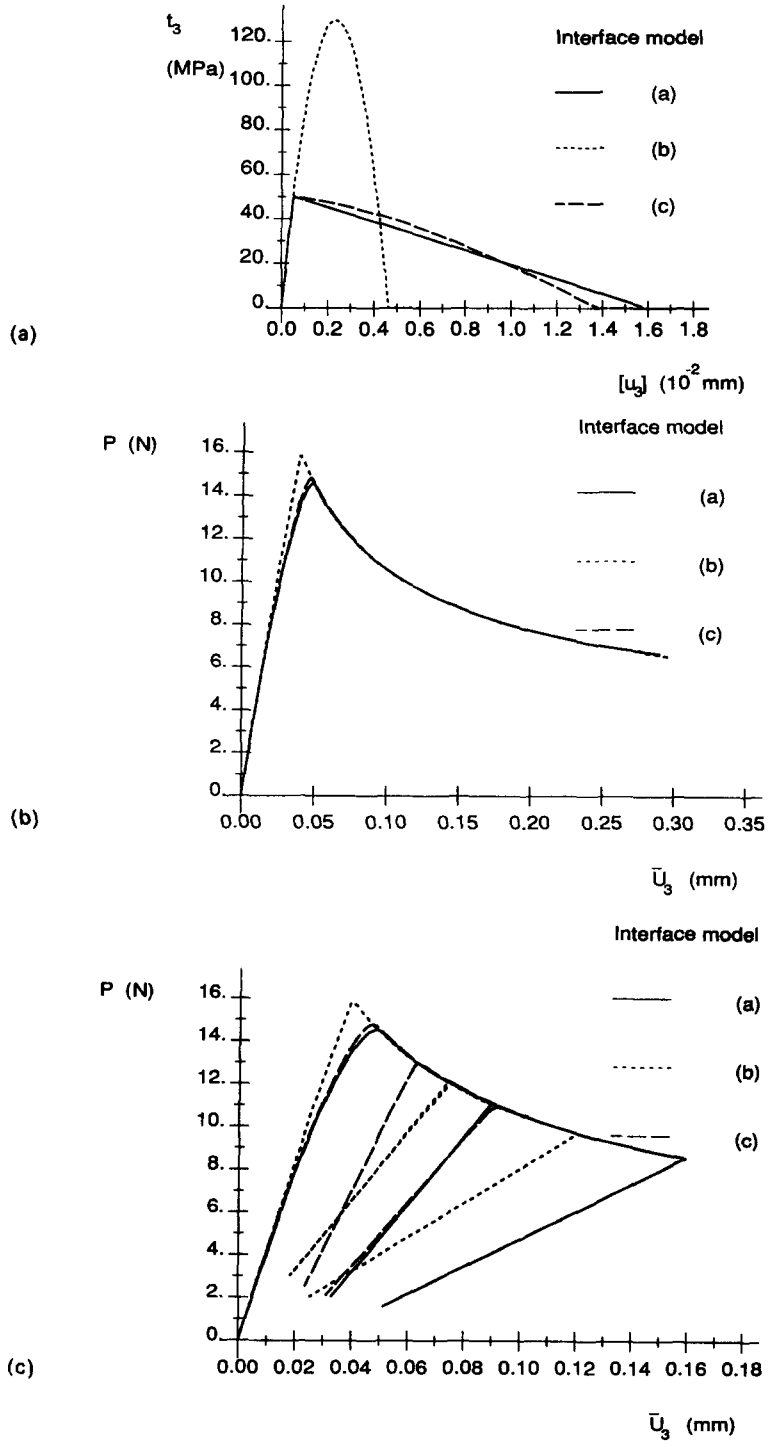

Fig. 15. Example 1, comparison of different interface models. (a) Uniaxial responses of interfacial models. (b) Load versus displacement for monotonously progressing fracture. (c) Load versus displacement for fracture progression with partial unloadings.

—model a

$$a_4 = 0\ \text{mm}^2\ \text{N}^{-1},\quad h = 1\ \text{mm}\ \text{N}^{-1},\quad b_3 = 0.4551 \times 10^{-3}\ \text{mm}^4\ \text{N}^{-2}$$

—model b

$$\gamma_3 = 0.06109.$$

In Fig. 17(a) the diagrams of load versus displacement at the extremum of the beam

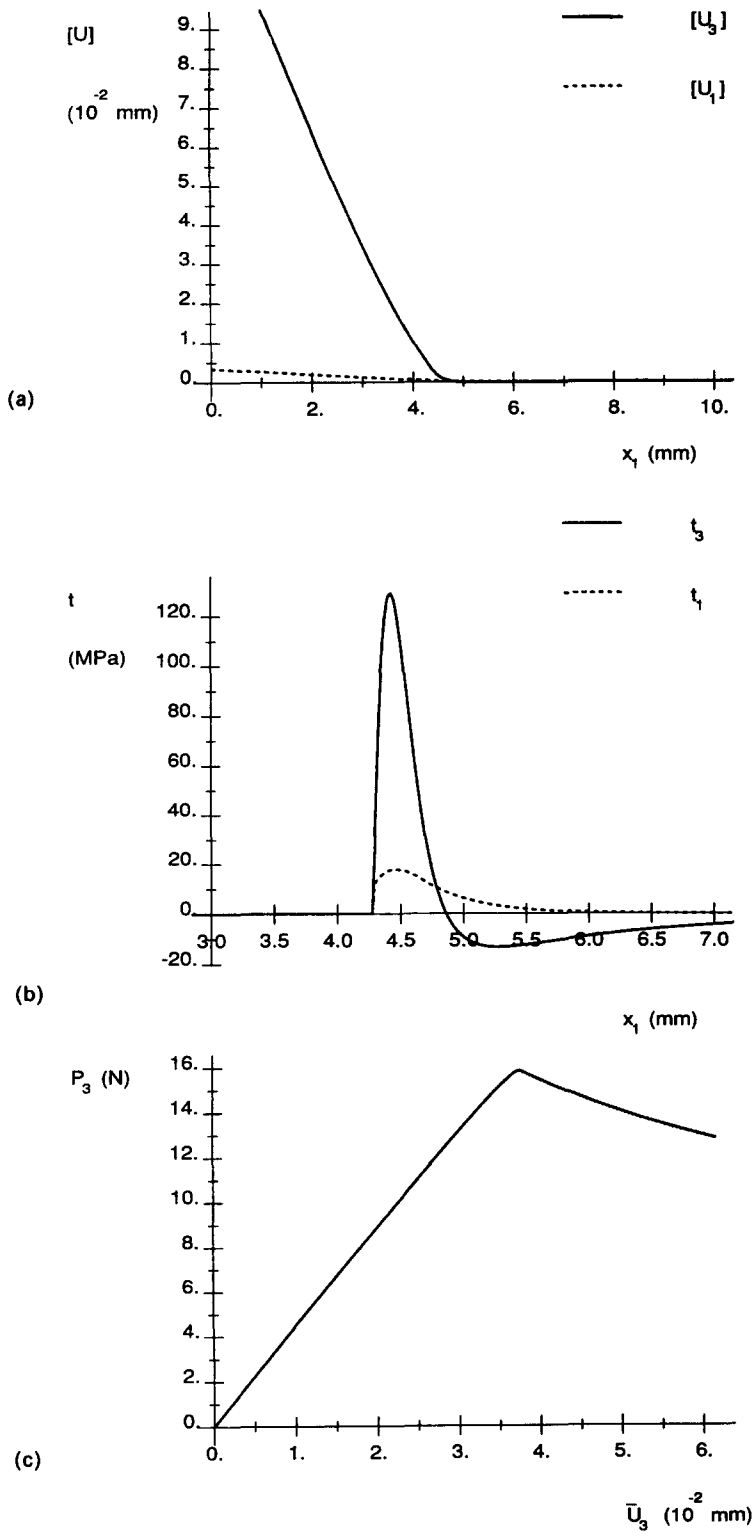

Fig. 16. Example 2. (a) Displacement discontinuities on half beam length. (b) Normal and shear stresses at crack tip. (c) Vertical load component versus vertical displacement component.

are reported for models a and b. In Fig. 17(b) a numerical analysis made with a coarser mesh (smallest element with 0.1 mm length) and model b is compared to experimental results taken from the load–displacement diagram reported in Ye (1992). The numerical results are in good agreement with the experimental ones; it is worth noticing that the only information used for identification of the interface model has been G_{Ic}.

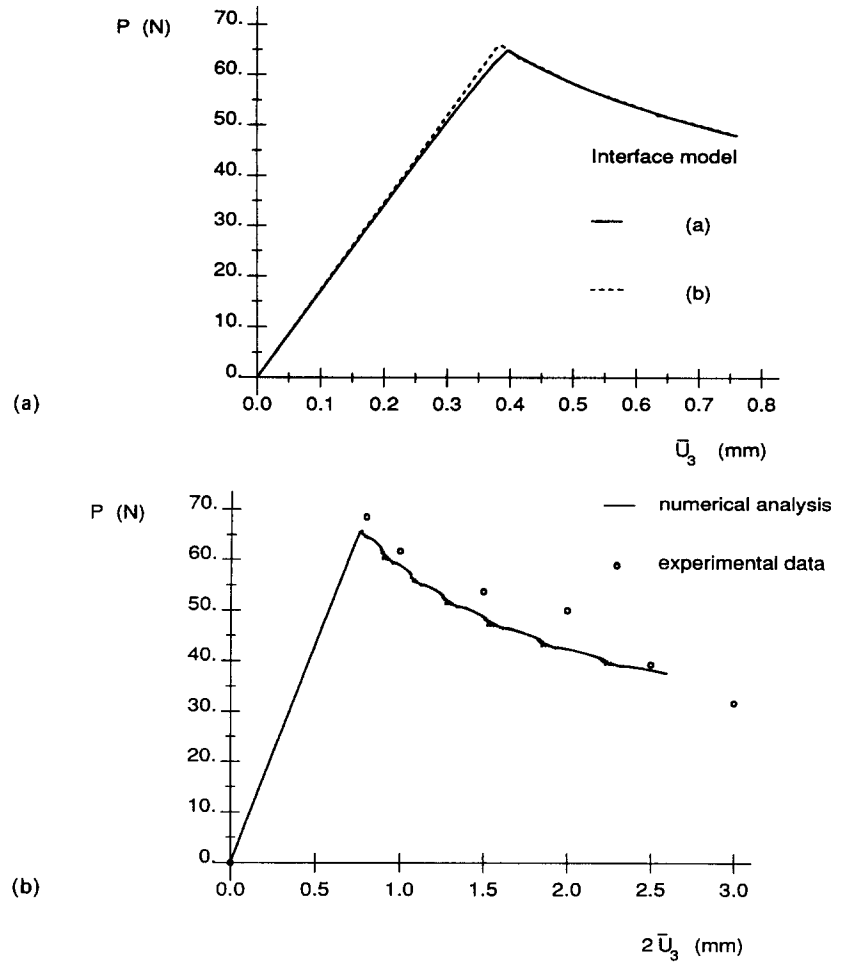

Fig. 17. Example 3. (a) Load versus displacement for two interface models. (b) Comparison of numerical and experimental results derived from Ye (1992).

8. CLOSING REMARKS

(i) The interface models proposed are suitable for mixed mode propagation. Also cyclic loading conditions can in principle be well simulated, but this requires further study and comparisons with experimental data. Among the proposed models, the elastic-damage model of Section 2.2 is the simplest one from a computational point of view. The elastic–plastic-damage model of Section 2.3 appears to be the more adequate for cyclic loading. The comparison in uniaxial situations can be judged from the numerical results of Section 7, while a more deep analysis is needed in order to compare the behaviour of the models in mixed-mode situations.

(ii) The identification procedure proposed makes use of the Critical Energy Release Rates obtained in Fracture tests as the most important parameters for interface models.

(iii) The validity of the schematization introduced for composite delamination has been confirmed, at least for progressive fracture propagation.

(iv) The algorithm for the numerical integration of interface laws appear to be adequate to the difficulties involved. A study of convergence of the iterative procedure proposed for the solution of the nonlinear system has to be made. Comparisons between different algorithms must be made. The numerical integration of elastic-damage models is straightforward; this fact represents a great advantage for these kind of models if cyclic behaviour is not really important.

(v) The algorithm for the solution of the boundary value problem is well suited for the analysis of fracturing processes, at least for the progression of a single fracture in pure and mixed modes.

Acknowledgements—This work has been done while the author was a foreign researcher at the Laboratoire de Mecanique et Technologie (LMT)-ENS Cachan, France. Thanks are given to all members of LMT, in particular to Professor P. Ladevèze who inspired and followed this work, to Professor O. Allix for helpful discussions and to Dr L. Daudeville. The results of this paper were established in the frame of a research project sponsored by MURST 40%. A grant from CNR (Italian National Research Council) is also gratefully acknowledged.

REFERENCES

Allix, O. (1989). Delaminage par la mécanique de l'endommagement. In *Calcule des Structures et Intelligence Artificielle* (Edited by J. M. Fouet, P. Ladevèze and R. Ohayon), Vol. 1, pp. 39–59. Pluralis, Paris.

Allix, O., Daudeville, L. and Ladevèze, P. (1991). Delamination and damage mechanics. In *Mechanics and Mechanisms of Damage in Composites and Multi-materials* (Edited by D. Baptiste). Mep, London.

Allix, O. and Ladevèze, P. (1992). Interlaminar interface modelling for the prediction of delamination. *Int. J. Compos. Struct.* **22**(4), 235–242.

Bažant, Z. P. and Oh, B. H. (1983). Crack band theory for fracture of concrete. *Materiaux et Constructions* **16**, 155–177.

Benallal, A., Billardon, R. and Doghri, I. (1988). An integration algorithm and the corresponding consistent tangent operator for fully coupled elastoplastic and damage equations. *Commun. Appl. Num. Meth.* **4**, 731–740.

Bottega, W. J. (1983). A growth law for propagation of arbitrary shaped delaminations in layered plates. *Int. J. Solids Structures* **19**, 1009–1017.

Brewer, J. C. and Lagace, P. A. (1988). Quadratic stress criterion for initiation of delamination. *J. Compos. Mater.* **22**, 1141–1155.

Broek, D. (1989). *The Practical Use of Fracture Mechanics*. Kluwer, Dordrecht.

Carpinteri, A. (1989). Decrease of apparent tensile and bending strength with specimen size: Two different explanations based on fracture mechanics. *Int. J. Solids Structures* **25**, 407–429.

Cedolin, L., Dei Poli, S. and Iori, I. (1987). Tensile behaviour of concrete. *J. Engng Mech. ASCE* **113**, 431–449.

Chen, Z. and Schreyer, H. L. (1990). A numerical solution scheme for softening problems involving total strain control. *Comput. Struct.* **37**, 1043–1050.

Comi, C., Corigliano, A. and Maier, G. (1991). Extremum properties of finite-step solutions in elastoplasticity with nonlinear mixed hardening. *Int. J. Solids Structures* **27**, 965–981.

Crisfied, M. A. (1981). A fast incremental/iterative solution procedure that handles snap through. *Comput. Struct.* **13**, 55–62.

Crisfield, M. A. and Shi, J. (1991). A review of solution procedures and path-following techniques in relation to the nonlinear finite element analysis of structures. In *Nonlinear Computational Mechanics: State of the Art* (Edited by P. Wriggers and W. Wagner), pp. 47–68. Springer, Berlin.

Daudeville, L. (1992). Une methode simplifiee pour l'analyse du delaminge des structures composites stratifiees. ph.D. thesis, Univ. Paris 6.

De Borst, R. (1987). Computation of post bifurcation and post-failure behaviour of strain-softening solids. *Comput. Struct.* **25**, 211–224.

Donaldson, S. L. (1988). Mode III interlaminar fracture characterization of composite materials. *Compos. Sci. Technol.* **31**, 225–249.

Frémond, M. (1987). Adhesion of solids. *J. Theoretical Appl. Mech.* **6**, 383–407.

Garg, A. C. (1988). Delamination—a damage mode in composite structures. *Engng Fract. Mech.* **29**, 557–584.

Hashin, Z. (1990). Thermoelastic properties of fiber composites with imperfect interfaces. *Mech. Mater.* **8**, 333–348.

Hillerborg, A., Modéer, M. and Petersson, P. E. (1976). Analysis of crack formation and crack growth in concrete by means of fracture mechanics and finite elements. *Cement and Concrete Research* **6**, 773–782.

Ju, J. W. (1989). On energy-based coupled elastoplastic damage theories: constitutive modeling and computational aspects. *Int. J. Solids Structures* **25**, 803–833.

Ladevèze, P. (1983). Sur une théorie de l'endommagement anisotrope. Internal Report No. 34. LMT-Cachan, France.

Ladevèze, P. (1986). Sur la mécanique de l'endommagement des composites. *JNC* **5**, 667–683.

Ladevèze, P. (1992). A damage computational method for composite structures. *Comput. Struct.* **44**, 79–87.

Laksimi, A., Benzeggagh, M. L., Jing, G., Hecini, M. and Roelandt, J. M. (1991). Mode I interlaminar fracture of symmetrical cross-ply composites. *Compos. Sci. Technol.* **41**, 147–164.

Lemaitre, J. (1984). How to use damage mechanics. *Nucl. Engng Des.* **80**, 233–245.

Lemaitre, J. (1992). Formulation de l'endommagement des interfaces. *C.R. Acad. Sc. Paris*, t. 315, Série II, pp. 1047–1050.

Lemaitre, J. and Chaboche, J. L. (1985). *Mécanique des Matériaux Solides*. Dunod, Paris.

Lene, F. (1986). Damage constitutive relations for composite materials. *Engng Fract. Mech.* **25**, 713–728.

Maier, G. (1968). On softening flexural behaviour in elastic–plastic beams (in Italian). *Rend. Ist. Lombardo, Classe Sci.* **A102**, 648–677 (English translation in *Studi e Ricerche* **8**, (1986), 85–117).

Maier, G., Cen, Z., Novati, G. and Tagliaferri, R. (1991). Fracture, path bifurcations and instabilities in elastic-cohesive-softening models: A boundary element approach. In *Fracture Processes in Concrete, Rock and Ceramics* (Edited by J. G. M. van Mier, J. G. Rots and A. Bakker), pp. 561–570. E&FN SPON, London.

Maier, G., Novati, G. and Cen, Z. (1992). Symmetric Galerkin boundary element method for quasi-brittle-fracture and frictional contact problems. *Comput. Mech.* (In press).

Pagano, N. J. (ed.) (1989). *Interlaminar Response of Composite Materials*. Composite Material Series, Vol. 5, Elsevier.

Perego, U. (1988). Explicit backward difference operators and consistent predictors for linear hardening elastic–plastic constitutive laws. *S. M. Arch.* **13**(2), 65–102.

Ramm, E. (1981). Strategies for tracing nonlinear responses near limit points. In *Nonlinear Finite Element Analysis in Structural Mechanics* (Edited by W. Wunderlich, E. Stein and K. J. Bathe), pp. 68–89. Springer, New York.

Riks, E. (1972). The application of Newton's method to the problem of elastic stability. *J. Appl. Mech.* **39**, 1060–1066.

Schellekens, J. C. J. and de Borst, R. (1992). Simulation of free edge delamination via finite element techniques. In *New Advances in Computational Structural Mechanics* (Edited by P. Ladevèze and O. C. Zienkiewicz), pp. 397–410. Elsevier, Amsterdam.

Schellekens, J. C. J. and de Borst, R. (1992). Application of anisotropic softening plasticity to mixed mode delamination in composites. *Proceedings of the Third International Conference on Computational Plasticity, Barcelona* (Edited by P. J. Owen, E. Oñate and E. Hinton). Pineridge Press.

Simo, J. C. and Ju, J. W. (1987). Stress and strain based continuum damage models—I. Formulation. *Int. J. Solids Structures* **23**, 821–840.

Simo, J. C. and Taylor, R. L. (1985). Consistent tangent operators for rate-independent elastoplasticity. *Comp. Meth. Appl. Mech. Engng* **48**, 101–118.

Suo, Z., Bao, G. and Fan, B. (1992). Delamination R-curve phenomena due to damage. *J. Mech. Phys. Solids* **40**, 1–16.

Wempner, G. A. (1971). Discrete approximations related to nonlinear theories of solids. *Int. J. Solids Structures* **7**, 1581–1589.

Ye, L. (1992). Evaluation of mode-I interlaminar fracture toughness for fibre-reinforced composite materials. *Compos. Sci. Technol.* **43**, 49–54.

APPENDIX

A.1. *Solution scheme for the plastic-damage corrector phase in the case of $t_{3_{n+1}}$ positive*

By eliminating from system (49)–(55) and (56a) (with equality sign) variables $[\mathbf{u}]^{e}_{n+1}$, $\mathbf{Y}_{n+1}$, χ_{n+1}, λ_{n+1} and $[\mathbf{u}]^{p}_{n+1}$ making use of eqns (49), (51)–(54) and (56a), the following six equation system is obtained:

$$\frac{1}{\tilde{K}_{i_{n+1}}}\tilde{t}_{i_{n+1}}+b_i\frac{\tilde{t}_{i_{n+1}}}{\sqrt{Y_{b_{n+1}}}}(h^{-1}(\sqrt{Y_{a_{n+1}}}+a_4\tilde{t}_{3_{n+1}}-1)-\lambda_n)=(1-d_{i_{n+1}})[u_i]^{e\,\mathrm{trial}}_{n+1} \tag{A1}$$

$$d_{i_{n+1}}=L_i(h(\lambda_{n+1})). \tag{A2}$$

In eqn (A1) $\tilde{t}_{in+1}$ and $\tilde{K}_i$ are *effective tractions* and *effective elastic stiffnesses* here defined as:

$$\tilde{t}_i=\frac{t_i}{(1-d_i)},\quad \tilde{K}_i=\frac{K_i}{(1-d_i)}\quad i=1,2,3. \tag{A3}$$

Note that scalars $Y_{a_{n+1}}$ and $Y_{b_{n+1}}$ can be considered as functions of effective tractions $\tilde{t}_{in+1}$ by making use of eqns (A3a) and (29). Hence for given damage variables $d_{i_{n+1}}$, eqns (A2) can be considered as a nonlinear system in the unknowns $\tilde{t}_{i_{n+1}}$. The system can be interpreted as a plastic corrector for an *effective elastic–plastic interface* with elastic stiffnesses $\tilde{K}_{in+1}$ where the input quantities are the *effective elastic trial displacement discontinuities* $(1-d_{in+1})[u_i]^{e\,\mathrm{trial}}_{n+1}$ while *effective plastic displacement discontinuities* $(1-d_{in+1})[u_i]^{p}_{n+1}$ are looked for. Equations (A1)–(A2) can be solved by an iterative procedure in which at each iteration the solution of the nonlinear system (A1) gives values of $\tilde{t}_{in+1}$ for fixed damage variables. A convergence control on the value of damage variables obtained at two subsequent interations can be used.

A.2. *Consistent tangent matrix in the case of positive $t_{3_{n+1}}$*

(1) Elastic unloading.

In this case the solution is given by the elastic predictor. The consistent tangent matrix reads:

$$\mathbf{J}=(\mathbf{I}-\mathbf{D}_{n+1})\mathbf{K}\equiv\mathbf{K}^{D}. \tag{A4}$$

In eqn (A4) $\mathbf{I}$ is the 3×3 identity matrix; $\mathbf{D}_{n+1}$ and $\mathbf{K}$ are 3×3 diagonal matrices with the component of principal diagonal given by $d_{i_{n+1}}$ and K_i respectively ($K_3=K_3^{+}$); $\mathbf{K}^{D}$ is here defined as the *secant* elastic-damage matrix.

(2) Elastic–plastic-damage loading.

$\mathbf{J}$ has to be found by differentiating with respect to variables $\mathbf{t}_{n+1}$, $\mathbf{d}_{n+1}$, λ_{n+1}, $[\mathbf{u}]_{n+1}$, $[\mathbf{u}]^{p}_{n+1}$, the following system of equations:

$$\mathbf{t}_{n+1}-\mathbf{K}^{D}([\mathbf{u}]_{n+1}-[\mathbf{u}]^{p}_{n+1})=\mathbf{0}, \tag{A5a}$$

$$F_{n+1}=F_{n+1}(\mathbf{t}_{n+1},\mathbf{d}_{n+1},\lambda_{n+1})=\sqrt{Y_{a_{n+1}}}+a_4\frac{t_{3_{n+1}}}{(1-d_{3_{n+1}})}-h(\lambda_{n+1})-1=0, \tag{A5b}$$

$$\Delta[\mathbf{u}]^{p}-\mathbf{r}(\mathbf{t}_{n+1},\mathbf{d}_{n+1})\Delta\lambda=\mathbf{0}, \tag{A5c}$$

$$\mathbf{d}_{n+1}-\mathbf{L}(\lambda_{n+1})=\mathbf{0}. \tag{A5d}$$

System (A5) has been obtained from relations (49)–(56) in the case of plastic-damage loading and for positive tractions $t_{3_{n+1}}$. The 3-components vectors $\mathbf{r}$ and $\mathbf{L}$ gather respectively the terms $b_i t_{i_{n+1}}/(1-d_{i_{n+1}})^2\sqrt{Y_{b_{n+1}}}$ and $L_i(h(\lambda_{n+1}))$. By computing derivatives of the system (A5) and after some calculations the following result is obtained:

$$\mathbf{J}=(\mathbf{I}+\mathbf{J}_1+\mathbf{J}_2)\mathbf{K}^{D}, \tag{A6}$$

$$\mathbf{J}_1\equiv-\frac{1}{D}(\mathbf{K}^{D}\mathbf{A}^{-1}\mathbf{r}^{D}+\partial\mathbf{L}\mathbf{K}[\mathbf{u}]^{e}_{n+1})\left(\frac{\partial F_{n+1}}{\partial\mathbf{t}}\right)^{T}_{n+1}, \tag{A7}$$

$$\mathbf{J}_2 \equiv \Delta\lambda\left\{\mathbf{K}^D\mathbf{A}^{-1}\left[\frac{1}{D}\mathbf{r}^D\left(\frac{\partial F_{n+1}}{\partial \mathbf{t}}\right)_{n+1}^T\mathbf{K}^D\mathbf{A}^{-1}-\mathbf{I}\right]+\frac{1}{D}\partial\mathbf{L}\mathbf{K}[\mathbf{u}]^e_{n+1}\left(\frac{\partial F_{n+1}}{\partial \mathbf{t}}\right)_{n+1}^T\mathbf{K}^D\mathbf{A}^{-1}\right\}\left(\frac{\partial \mathbf{r}}{\partial \mathbf{t}}\right)_{n+1}^T, \tag{A8}$$

$$D \equiv \left[\left(\frac{\partial F_{n+1}}{\partial \mathbf{t}}\right)_{n+1}^T\mathbf{K}^D\mathbf{A}^{-1}\mathbf{r}^D+\left(\frac{\partial F_{n+1}}{\partial \mathbf{t}}\right)_{n+1}^T\partial\mathbf{L}\mathbf{K}[\mathbf{u}]^e_{n+1}-\left(\frac{\partial F_{n+1}}{\partial \mathbf{d}}\right)_{n+1}^T\left(\frac{\partial \mathbf{L}}{\partial\lambda}\right)_{n+1}-\left(\frac{\partial F_{n+1}}{\partial\lambda}\right)_{n+1}\right], \tag{A9}$$

$$\mathbf{A} \equiv \mathbf{I}+\Delta\lambda\left(\frac{\partial \mathbf{r}}{\partial \mathbf{t}}\right)_{n+1}^T\mathbf{K}^D, \tag{A10}$$

$$\mathbf{r}^D \equiv \mathbf{r}-\Delta\lambda\left[\left(\frac{\partial \mathbf{r}}{\partial \mathbf{t}}\right)_{n+1}^T\partial\mathbf{L}\mathbf{K}[\mathbf{u}]^e_{n+1}+\left(\frac{\partial \mathbf{r}}{\partial \mathbf{d}}\right)_{n+1}^T\left(\frac{\partial \mathbf{L}}{\partial\lambda}\right)_{n+1}\right], \tag{A11}$$

$$\partial\mathbf{L} \equiv \text{diag.}\left[\left(\frac{\partial L_i}{\partial\lambda}\right)_{n+1}\right]. \tag{A12}$$

Equations (A6)–(A12) give the consistent tangent matrix $\mathbf{J}$ as the sum of three terms. The first one is the matrix for the unloading case (the secant matrix). The second and third terms represent the corrections for the plastic-damage loading case. Note that if $\Delta\lambda$ goes to the zero matrix $\mathbf{A}$ [eqn (A10)] reduces to the identity, vector $\mathbf{r}^D$ [eqn (A11)] coincides with $\mathbf{r}$, matrix $\mathbf{J}_2$ [eqn (A8)] goes to zero and the tangent matrix J reads:

$$\lim_{\Delta\lambda\to 0}\mathbf{J} = \left[\mathbf{I}-\frac{1}{D}(\mathbf{K}^D\mathbf{r}+\partial\mathbf{L}\mathbf{K}[\mathbf{u}]^e_{n+1})\left(\frac{\partial F_{n+1}}{\partial \mathbf{t}}\right)_{n+1}^T\right]\mathbf{K}^D. \tag{A13}$$

The above expression for $\mathbf{J}$ coincides with that for the continuum tangent operator which can be obtained directly from the relations (2), (8) and (27)–(32). It is also worth noticing that $\mathbf{J}$ is in the general case nonsymmetric. When a class of models of the kind of example a in Section 2 is considered (elastic–plastic-softening), the matrix $\mathbf{K}^D$ coincides with $\mathbf{K}$, matrix $\partial\mathbf{L}$ goes to zero and the elastic–plastic consistent tangent matrix is recovered from eqns (A6)–(A12). The tangent modulus in the case of an elastic-damage class of models (model b in Section 2) is obtained for vectors $\mathbf{r}$ and $\mathbf{r}^D$ which go to zero. Note that in this last case the consistent tangent matrix given by eqn (A6) coincides with the continuum, tangent modulus given by eqn (A13).

A.3. *Iterative solution for system* (66)

At each iteration $(j+1)$ the equations to solve are (66) and the linearization of (66a) around the estimate at the preceding iteration j:

$$\mathbf{q}(\mathbf{U}_{j+1})-\mu_{j+1}\mathbf{P} \cong \mathbf{q}(\mathbf{U}_j)-\mu_{j+1}\mathbf{P}+\mathbf{Q}_j(\mathbf{U}_{j+1}-\mathbf{U}_j) = 0, \tag{A14a}$$

$$\mathbf{c}^T\mathbf{B}^*(\mathbf{U}_{j+1}-\mathbf{U}_n)-\alpha = 0. \tag{A14b}$$

In the above equations the step index $(n+1)$ has been dropped for notation convenience.

Matrix $\mathbf{Q}_j$ in eqn (A14a) is used for the linearization and can be chosen in different ways. If $\mathbf{Q}_j$ coincides with the tangent matrix of the structure, i.e. $\mathbf{Q}_j = (\partial\mathbf{q}/\partial\mathbf{U})_j^T$ the Newton–Raphson method is obtained. $\mathbf{Q}_j$ can also be chosen equal to the tangent matrix computed at the beginning of the step, i.e. $\mathbf{Q}_j = (\partial\mathbf{q}/\partial\mathbf{U})_n^T \forall j$, or equal to the secant matrix or even to the initial elastic stiffness matrix. The quadratic asymptotic rate of convergence of the Newton–Raphson method can be obtained only if the derivative of the function $\mathbf{q}(\mathbf{U})$ is computed by considering the consistent tangent matrix for the numerically integrated constitutive law of the interfaces, derived in Section 5. For the first iteration of the procedure, use is made of results obtained at the end of the last step. The iteration procedure is stopped when the following conditions are satisfied:

$$\|\mathbf{U}_{j+1}-\mathbf{U}_j\| \leqslant \text{TOL}_U\|\mathbf{U}_1-\mathbf{U}_n\|, \quad \|\mu_{j+1}\mathbf{P}-\mathbf{q}(\mathbf{U}_j)\| \leqslant \text{TOL}_\mu\|\mu_1\mathbf{P}-\mathbf{q}(\mathbf{U}_n)\|. \tag{A15}$$

In eqns (A15) the 2-norm is inferred, TOL_U and TOL_μ are two tolerance parameters. The above convergence conditions are equivalent to those proposed by Chen and Schreyer (1990). The first condition (A15a) controls the changement of displacements from one iteration to the following, while the second (A15b) controls the value of residual forces.

It has to be observed that the first step of the analysis is to be done by following another strategy, for instance by imposing a value of load parameter μ which is below the elastic limit.

The value of load parameter μ_{j+1} is found after substitution of $\mathbf{U}_{j+1}$ obtained by the first equation (A14a) in the second equation (A14b):

$$\mathbf{U}_{j+1} = \mathbf{U}_j+\mathbf{Q}_j^{-1}(\mu_{j+1}\mathbf{P}-\mathbf{q}(\mathbf{U}_j)), \tag{A16a}$$

$$\mu_{j+1} = \frac{\mathbf{c}^T\mathbf{B}^*\mathbf{Q}_j^{-1}\mathbf{q}(\mathbf{U}_j)}{\mathbf{c}^T\mathbf{B}^*\mathbf{Q}_j^{-1}\mathbf{P}} \quad (j+1)>1, \quad \mu_1 = \frac{\alpha+\mathbf{c}^T\mathbf{B}^*\mathbf{Q}_n^{-1}\mathbf{q}(\mathbf{U}_n)}{\mathbf{c}^T\mathbf{B}^*\mathbf{Q}_n^{-1}\mathbf{P}}. \tag{A16b,c}$$

To derive eqns (A16b, c) use has been made of the fact that eqn (A14) also holds at iteration $j>0$ and that $\mathbf{U}_{j=0} = \mathbf{U}_n$.